Geomorphology 414 (2022) 108376

Contents lists available at ScienceDirect

Geomorphology

journal homepage: www.journals.elsevier.com/geomorphology

Geomorphic and sedimentary signatures of catastrophic glacier detachments: A first assessment from Flat Creek, Alaska

Mylène Jacquemart [a,b,c,*], Ethan Welty [d], Matthias Leopold [e], Michael Loso [f], Lia Lajoie [f,g], Kristy Tiampo [c]

[a] Laboratory for Hydraulics, Hydrology, and Glaciology (VAW), ETH Zurich, Zurich, Switzerland
[b] Swiss Federal Institute for Forest, Snow, and Landscape Research (WSL), Birmensdorf, Switzerland
[c] Cooperative Institute for Research in Environmental Sciences (CIRES), University of Colorado, Boulder, USA
[d] Department of Geography, University of Zurich, Zurich, Switzerland
[e] School of Agriculture and Environment, University of Western Australia, Perth, Australia
[f] Wrangell-St. Elias National Park and Preserve, Copper Center, USA
[g] Department of Geoscience, University of Montana, Missoula, MT, USA

ARTICLE INFO

Keywords:
Glacier detachments
Land-system model
Natural hazards
Climate change

ABSTRACT

Large-volume detachments of low-angle mountain glaciers involve the sudden mobilization of large amounts of glacier ice and lithic material in long-runout mass flows. Scientific investigations of these events have only recently brought to light their global occurrence and the similarities in the conditions under which they occur. While this recent research suggests that glacier detachments may become more frequent in a warming climate, a long-term record is largely lacking. Knowledge of the geomorphic signatures of glacier detachments could help establish such a record. Here, we present the first geomorphic and sedimentary assessment of a glacier detachment deposit. We investigate the landscape impacts of the Flat Creek glacier detachments in Alaska's St. Elias mountains through a combination of remote sensing analyses, field observations, Electrical Resistivity Tomography, and grain size and grain orientation analyses. From these data, we outline a land-system model that may help identify past glacier detachments elsewhere. Some of the most distinguishing features we documented were large bodies of buried ice-conglomerates, a rapid response of the remnant glacier ice, clusters of small-scale thermokarst ponds, countless molards, parallel striations etched into the hillslope and individual clasts, and a very long runout distance. We assess these features in terms of their longevity in the landscape and compare them to what has been described at glacier detachment sites elsewhere. Finally, we discuss to what extent glacier detachment deposits can be distinguished from deposits left by rock(−ice) avalanches, debris flows, and surging glaciers, and show that a differentiation is possible if detailed field investigations are undertaken.

1. Introduction

Sudden large-volume detachments of low-angle mountain glaciers are rare but highly destructive events that have recently received increased scientific attention, partly because they are suspected to become more frequent in a warmer climate. The first extensively documented event, the 2002 detachment of Kolka Glacier in the Russian Caucasus, killed over more than 120 persons (Haeberli et al., 2004; Evans et al., 2009). The 2016 detachments of two neighboring glaciers in Tibet's Aru Range (Kääb et al., 2018; Gilbert et al., 2018) reignited interest in these unusual events and inspired the detailed investigation of several similar incidents: the 2007 Leñas Glacier detachment in Argentina (Falaschi et al., 2019), the 2013 and 2015 Flat Creek Glacier detachments in Alaska (Jacquemart and Loso, 2019; Jacquemart et al., 2020), and several detachments in Tajikistan's Petra Pervogo and Tibet's Amney Machen ranges (Paul, 2019; Leinss et al., 2021). While several authors have raised the possibility that glacier detachments – or at least their frequent occurrence in recent years – may be a direct consequence of human-driven climate change (Kääb et al., 2018; Gilbert et al., 2018; Jacquemart et al., 2020), evidence of past glacier detachments is also coming to light. A recent compilation documents 28 confirmed or suspected glacier detachments dating back as far as 1776, eight of which predate the era of satellite and aerial observation (Kääb et al., 2021).

* Corresponding author at: Laboratory for Hydraulics, Hydrology, and Glaciology (VAW), ETH Zurich, Zurich, Switzerland.
E-mail address: jacquemart@vaw.baug.ethz.ch (M. Jacquemart).

https://doi.org/10.1016/j.geomorph.2022.108376
Received 11 February 2022; Received in revised form 15 July 2022; Accepted 16 July 2022
Available online 22 July 2022
0169-555X/© 2022 The Author(s). Published by Elsevier B.V. This is an open access article under the CC BY license (http://creativecommons.org/licenses/by/4.0/).

Glacier detachments – as we use the term in this publication – share an intriguing number of similarities. In each case, the tongue of a valley glacier with a modest slope (10° to 20°) suddenly detached and turned into a large (1×10^6 m^3 to 100×10^6 m^3) and highly-mobile icy (and sometimes debris-rich) mass flow. All detached glaciers overlaid fine-grained and/or weak, highly-erodible beds (Kääb et al., 2018). With only one exception, the detachments occurred in regions with numerous surging glaciers; some detached glaciers had a history of surging (e.g., Kolka, Petra Pervogo) or displayed a surgelike acceleration or mass redistribution in the months or weeks before their detachment (e.g., Aru, Flat Creek) (Jacquemart et al., 2020; Kääb et al., 2021; Leinss et al., 2021).

Despite these similarities, the exact mechanisms driving glacier detachments remain somewhat obscure. Liquid water has been shown to exert critical control on such events through a reduction of the glacier's basal friction (Gilbert et al., 2018). Large amounts of liquid water, as well as frictional heating, have also been invoked to explain the unusually large runout distances that all known glacier detachments manifest (Kääb et al., 2018). The Aru and Flat Creek detachments have been further linked to a polythermal glacier structure, in which a cold-ice tongue prohibited drainage and led to high subglacial water pressures. However, several glacier detachments have also occurred in warmer climates, where glaciers are presumed temperate, so a polythermal glacier does not appear to be a requirement (Kääb et al., 2018; Falaschi et al., 2019; Leinss et al., 2019).

These observations suggest that a climate-change induced increase in meltwater or precipitation may be making glacier detachments more common, but a record that stretches back to before the satellite era is necessary to establish an increase in frequency. Old aerial photographs, declassified spy satellite images, and historic accounts have helped to identify some possible past events (Kääb et al., 2021). In the absence of such direct evidence, however, it has yet to be determined whether we can correctly identify past glacier detachments solely from the geomorphic and sedimentary features they leave behind.

The need to identify past events in the geologic record in order to establish their historic frequency is common to the study of all rare and extreme events. To overcome this challenge for landslides, the scientific community has developed facies models that describe the typical sedimentary features of rock-avalanche and landslide deposits. These facies models have been used to identify landslide and rock avalanche deposits, determine the origin and extent of the mass movements, and even reconstruct their kinematics and runout dynamics (Dufresne and Davies, 2009; Shugar and Clague, 2011; Dufresne et al., 2018). Similarly, Evans and Rea (1999) described a land-system model for identifying evidence of past glacier surges based on various landforms, sedimentologic and stratigraphic features. We believe that building a similar land-system model for glacier detachments can help identify past glacier detachments in the landscape.

At first glance, glacier detachment deposits may resemble the long-runout rock-avalanche and debris-flow deposits found in periglacial environments. Additionally, glacier detachments tend to occur in regions with many surge-type glaciers. The rapid advances of such glaciers by up to tens of meter per day can carry or push forward large amounts of sediment and debris (Sevestre and Benn, 2015; Benn et al., 2019) and leave behind conspicuous glaciotectonic deposits (Evans and Rea, 1999). It is therefore important that our land-system model can help distinguish glacier detachment deposits from all three of these processes. However, with few known glacier detachments, and no detailed analysis of their deposits, such a model is clearly lacking.

To help determine the distinguishing features of glacier detachment deposits, and estimate how these may be preserved in the geologic record, we present – to our knowledge – the first in-depth investigation of a glacier detachment deposit. The 2013 and 2015 Flat Creek glacier detachments have been reconstructed in detail (Jacquemart et al., 2020); their deposits therefore offer an ideal natural laboratory from which to build this knowledge.

We describe the Flat Creek deposits with aerial and satellite image analysis, field observations, electrical resistivity tomography (ERT), as well as measurements of grain size and grain orientations. From this description, we develop a land-system model for glacier detachment deposits. Then, we apply this land-system model to a large lobate deposit in an adjacent drainage to determine whether it originated from a glacier detachment, a glacier surge, a rock(−ice) avalanche, or some other process. Finally, to the extent possible, we compare our findings with the descriptions of other deposits found in the literature. Our findings are a crucial first step towards reconstructing the long-term history of glacier detachments, which, in turn, are needed to inform present-day hazard management in mountain regions.

2. Study site

Flat Creek is a small, informally-named glacierized drainage in the eastern part of Wrangell-St. Elias National Park and Preserve (Fig. 1), a region that is home to numerous surge-type glaciers. The Flat Creek drainage extends from roughly 1000 m above sea level (asl), at the confluence with the White River, to about 2700 m asl at the top of a glaciated cirque. Flat Creek glacier occupied a central trough in the NNE-facing basin and was flanked by smaller and steeper glaciers on either side. Many of the catchments on the northern edge of the range are populated with similarly small glaciers, while very large glaciers dominate the range further south, several of which are surge-type glaciers. There is no evidence that Flat Creek glacier has a history of surging, but the glacier in the drainage immediately to the west of Flat Creek surged in the 1970s and again between 2012 and 2014 (Jacquemart et al., 2020).

Situated in the rain shadow of the St. Elias Mountains, the catchment receives only ~350 mm of precipitation annually. The mean annual air temperature at 2000 m asl is around −12 °C (Jacquemart et al., 2020). In agreement with a global permafrost model (Obu et al., 2019), ground temperature and ERT measurements indicate that permafrost is continuous in the upper part of the valley (above 1800 m asl) and discontinuous-to-sparse on the alluvial fan (below 1600 m asl). Due to these cold and dry conditions, many of the region's small glaciers, including the former Flat Creek glacier, are assumed to be polythermal (see Jacquemart et al., 2020 for details).

Geologically, the region is mostly covered by Quaternary glacial and fluvial deposits which are sourced primarily from volcanic and metamorphosed sedimentary rocks (Wilson et al., 2015). The glacierized headwall of the Flat Creek drainage lies in the Hasen Creek Formation, which is made up of highly incompetent, thin-bedded, Permian-age sand- and siltstones (Fig. 1). The right-lateral Totschunda fault runs from NE to SW just south of the Flat Creek drainage (Schwartz et al., 2012), and the headwall shows evidence of fault-related bedrock fracturing. Just downstream of the headwall, the lithology changes unconformably to the submarine-to-subaerial basalts of the Nikolai Greenstone formation (Upper/Middle Triassic; MacKevett, 1978). The pre-detachment morphology of the Flat Creek alluvial fan closely resembled that of neighboring drainages (see Appendix A, Fig. A4): abandoned river channels and vegetation in various stages of regrowth are evidence of regular debris flows (Hungr et al., 2014). The debris is likely sourced from the many steep ravines that deliver loose material to the main drainage channels, and is subsequently transported onto the fans during rainfall and snowmelt events.

Three glacier detachments – in 2013, 2015, and 2016 – have impacted about 25 % (9 km^2) of the Flat Creek watershed, and are thoroughly described in Jacquemart et al. (2020). In 2013, 6.8 to 11.1 million m^3 of ice and lithic material were released and an additional $1.9 \pm 0.7 \times 10^6$ m^3 were eroded from the channel, resulting in deposits of $9.1 \pm 1.1 \times 10^6$ m3. In 2015, the release volume involved 17.6 to 20.1 million m^3, an additional $2.8 \pm 0.4 \times 10^6$ m^3 were entrained and the depositional volume amounted to $17.5 \pm 1.0 \times 10^6$ m^3. Distinct deposits are evident from 1 km to 11 km downstream of the former glacier

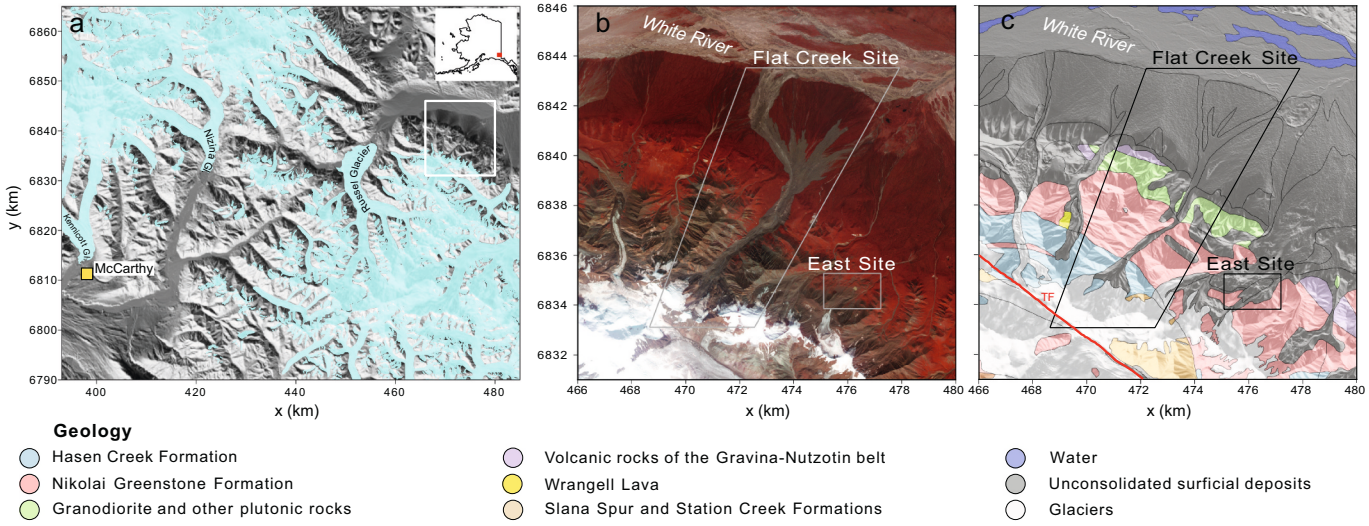

Fig. 1. (a) Location of the Flat Creek watershed on the northern edge of the St. Elias Mountains in Wrangell St. Elias National Park and Preserve, roughly 80 km NE of McCarthy, Alaska. The white rectangle indicates the extent of subsequent panels. Glacier coverage (light blue) is from the Randolph Glacier Inventory (RGI; RGI Consortium, 2017). (b) False color image of the study area and sites investigated in this study (Planet image from 201607-31; © Planet Team, 2017). (c) Geologic map of the study region from the United States Geological Survey (USGS); the main trace of the Totschunda Fault (TF) is drawn in red (Wilson et al., 2015).

terminus (Fig. 1). For the first 4 km, the mass flows remained largely contained within the river channel (henceforth, the "channelized reach"). Once on the alluvial fan, they spread ice and debris across large swaths of the previously vegetated floodplain and buried about 4 km^2 of old-growth White Spruce (*Picea glauca*) forest (Fig. 2). The 2016 release involved $4.7 \pm 0.2 \times 10^6$ m^3 (Kääb et al., 2021). Despite the relatively low slope, the 2013 and 2015 detachments attained very high mean velocities of ~30 ms^{-1} (Jacquemart et al., 2020) near the end of the channelized reach. By comparison, the 2016 event only reached around 10 ms^{-1} (Kääb et al., 2021).

About 4.5 km east of the Flat Creek drainage (Fig. 1), an older deposit with visible ice blocks superficially resembles the Flat Creek detachment deposits. Could this drainage (referred to as "East Site" in this paper) have experienced a glacier detachment sometime in the past? A small, intact glacier with a geometry similar to that of the pre-detachment Flat Creek Glacier lies 1 km upstream of the deposit. Satellite images reveal that the deposit predates the era of modern Earth observation, making this site a good place to subject our land-system model to its first application.

3. Methods and data

To develop a land-system model of glacier detachments, we documented the morphologic and sedimentary structures of the Flat Creek deposit. We used remote sensing data acquired between 2012 and 2019 and field observations – including ERT surveys, grain-size distributions, and clast orientations – gathered in 2018 and 2019. A summary of all datasets is shown in Table 1. Fig. 2 provides an overview of our measurements and mapped landforms.

3.1. Image interpretation and DEM differencing

We used high-resolution satellite images (Planet, Ikonos), orthophotos acquired on overflights in 2016 and 2019, structure-from-motion (SfM) DEMs from these same overflights, as well as regional DEMs (ArcticDEM, Alaska IFSAR) to characterize the landscape changes caused by the glacier detachments. An overview of all datasets is shown in Table 1.

The 2012 Alaska IFSAR DEM served as our pre-event reference of surface elevations, and we aligned all subsequent DEMs to this reference by minimizing the slope- and aspect-dependent offsets that result from misaligned DEMs in elevathion difference maps following Nuth and Kääb (2011). After alignment, a mean elevation increase (around 0.3 m) remained over large parts of the deposits. Neither vegetation regrowth nor differences in snow cover can explain this height increase. Rather, we would expect a lowering of the surface, as the deposits settle and remaining ice melts. We therefore interpret this offset as a systematic error resulting from the DEM generation and subtract it from the elevation change map. This correction brings out the features of the changing surface morphology more clearly, but does not completely eliminate the issue. However, it has no impact on the conclusions we draw from the data. We also used the DEMs and satellite images to measure the horizontal runout distance (L) and fall height (H) of each detachment, from the highest point of the release to the lowest point of the runout, and then used these to compute the angle of reach (termed Fahrböschung by Scheidegger (1973)) as arctan(H/L).

The SfM-based orthophotos – available at resolutions of 0.25 m and 0.2 m for 2016 and 2019, respectively – were the basis for the geomorphic mapping. In order to show the full breadth of the features visible in these data, we have made them publicly available. The orthophotos, as well as the geometries of mapped features, are available at https://doi.org/10.3929/ethz-b-000558233.

3.2. Field observations

We documented the morphology and characteristics of the detachment deposits on two field campaigns during the summers of 2018 and 2019. Along roughly 11 km from the source to the distal edge of the Flat Creek deposit, we mapped and characterized superficial deposit features (e.g. hummocks, levees), changes to the river channel, ice presence, tree damage, clast size and angularity, trimlines and superelevation heights, erosion and deposition, and, from a safe distance, conditions in the glacier cirque. These observations provide essential context for interpreting the remote sensing and geophysical data.

3.3. Electrical resistivity tomography (ERT)

To characterize the internal structure of the debris deposits and assess the remaining ice content, we conducted 15 ERT surveys along transects measuring 20 m to 200 m; 11 at Flat Creek – three of which were for permafrost assessment outside the deposit – and 4 at the East Site. We chose the measurement sites to include both the absence and

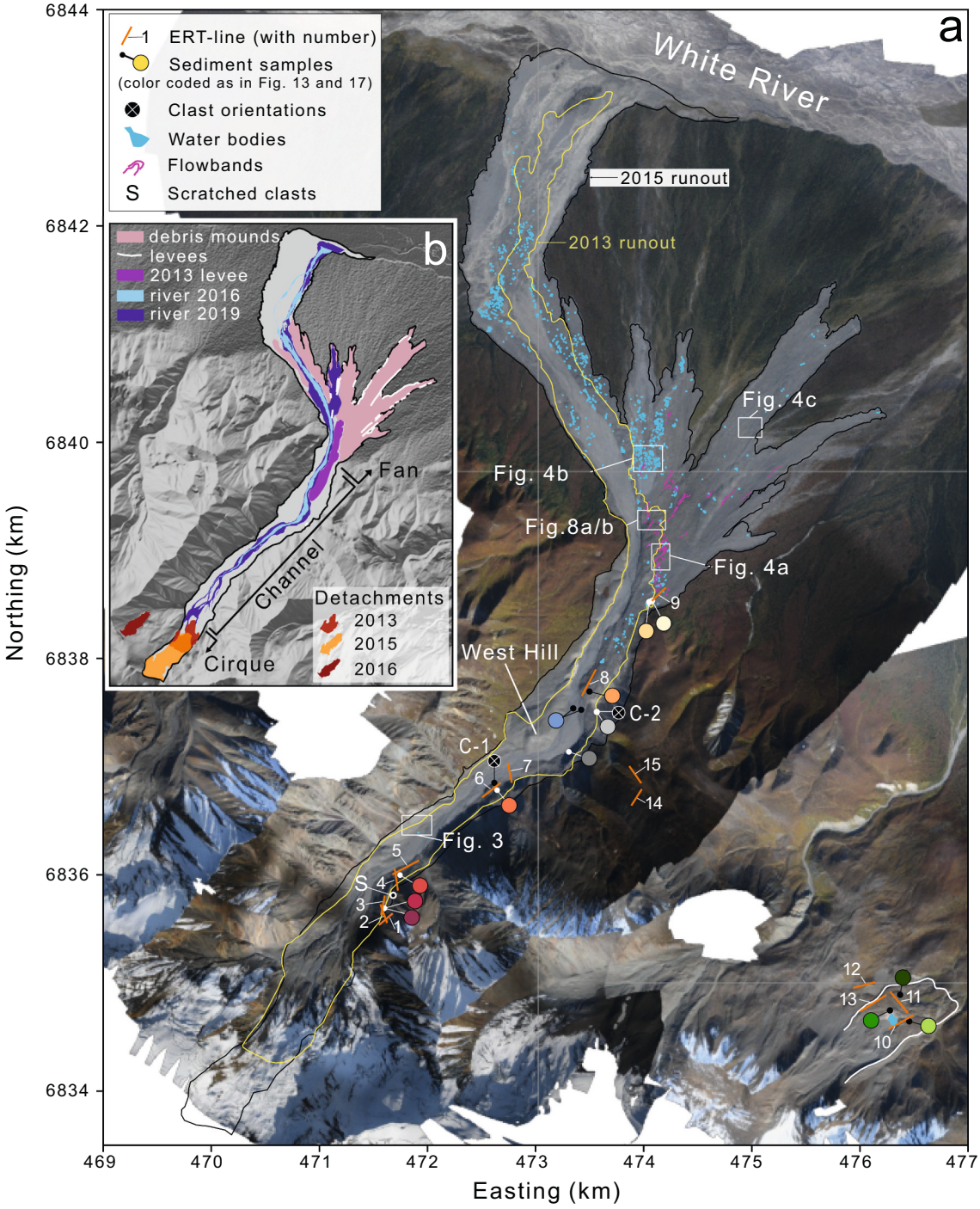

Fig. 2. Overview of sampling locations and mapped features. Panel a) shows mapped features and locations of ERT surveys, locations where grain sizes and orientations were sampled, and the 2013 and 2015 runouts overlaid on the 2019 orthophoto mosaic. The sediment sampling locations are colored to correspond to the plotted grain size distributions in Figs. 13 and 17. The numbered ERT lines correspond to the results presented in Figs. 12 and 16. Panel b) outlines distinct features described in the paper: the three detachment zones (2013, 2015, and 2016) in the cirque, the channelized reach and alluvial fan, the changing river channel, and areas with levees and hummocks.

presence of pooling water (suggesting the presence of melting ice), at increasing distances from the source area. Sites also needed to be at a safe distance from the release zone, not be overly steep, and represent a variety of deposit thicknesses.

We used a multi-electrode system from Lippman Geophysical Instruments (4punktlight hp) with up to 40 electrodes and a combined Wenner and dipole-dipole array. The measurement frequency of 5 Hz and applied currents of 0.1 mA to 5.0 mA resulted in measured voltages of 1 mV to 108 mV. Each point was measured at least three times and averaged. Points exceeding 2 % difference between measurements were measured five times and points exceeding 5 % were removed. We used the RES2DINV software (Loke, 2006) to invert the apparent resistivity values and produce a 2-dimensional model of the specific electric resistivity of the subsurface. A least-squares inversion was chosen to compile specific resistivity models. The models reached the desired 2 % convergence limit usually after six to seven iterations. This yielded differences between measured and modeled apparent resistivity sections of 1.8 to 6.1 % which is well within the accepted value range of data

Table 1
Data products used for DEM differencing and image analysis in this study.

Data type	Source	Acquisition date	Resolution (m)
Orthophoto	Ikonos	2009-07-13	0.5
Optical image	Planet Labs	2012-08-15	5
		2013-08-11	
		2015-07-25	
		2015-08-13	
Optical image	SfM 2016	2016-06-01	0.25
Optical image	SfM 2019	2019-08-30	0.2
DEM	Alaska IFSAR	Aug./Sep. 2012	5
DEM	Arctic DEM	2014-10-12	2
		2016-03-13	
DEM	SfM 2016	2016-06-01	0.5
DEM	SfM 2019	2019-08-30	0.2

misfit (Hauck and Vonder Mühll, 2003; Leopold et al., 2013).

3.4. Grain size analysis

We collected 14 sediment samples and used a combined field and laboratory approach to determine their grain size distributions. At Flat Creek, we collected seven samples from the interior of the detachment deposits and at increasing distances from the release zone, two from an area where the river had reworked the deposits, and two from hillslopes outside the deposits (regolith not affected by the detachments). At the East site, we collected two samples from the shore of a lake with visible ice remnants and one from the front of the lobate deposit (Fig. 2).

At each location, we excavated roughly 9000 cm^3 of sediment from the interior of the deposit (~30 cm below the surface) and weighed the sample with a handheld digital scale. We then sieved the sample to separate grains with diameters larger than 21 mm, weighed these large grains, and spread them out on a white plastic sheet of known size. We photographed the sheet with a handheld camera from a central location and constant distance to the ground. The outlines of the grains in each photograph were traced automatically (by converting each photograph to a binary image using Otsu's method (Otsu, 1979), after which we reviewed and corrected the outlines manually as needed. In each photograph, the lengths in pixels of the four sides of the sheet were used to compute the average size of each pixel in millimeters, which we used to convert the pixel area of each grain outline to physical units. Assuming a perfect sphere and constant density, we calculated the relative contribution of each grain to the total weight of the large fraction for that sample.

The grains between 2 mm and 21 mm (330 g to 775 g) were brought back to the lab, freeze dried, and dry-sieved through 16 mm, 8 mm, 4 mm and 2 mm sieves to record the relative weights of the four fractions.

The grain size distribution of the smallest fraction (<2 mm) was determined using laser diffraction. We used a sample splitter to extract a representative 1 g to 1.5 g from each sample and removed any organic material by subjecting all samples to two 5 mL treatments of hydrogen peroxide. We then added 8 mL to 10 mL of magnesium chloride to aid settling and siphoned off the excess water. The samples were centrifuged for 20 min before being treated with 20 mL of sodium metaphosphate to disperse any clumped particles. Finally, we ran 10 to 15 measurements on a Malvern Master Sizer 3000 and took the median value of all measurement runs.

3.5. Clast orientations

We measured clast orientations in two different outcrops at Flat Creek. The first outcrop was a thick detachment deposit in the middle of the channelized reach (C-1 Fig. 2). The second outcrop was located along the edge of the detachment deposit, where a gully incised into a thin detachment deposit (0.5 m thick) and the underlying hillslope (C-2 in Fig. 2), allowed us to sample clasts from both layers in one location.

At each outcrop, we excavated a vertical cross-section (roughly 1x1 m) and randomly extracted clasts to record the horizontal heading (azimuth angle) of their long axis relative to the dip direction of the deposit surface (in six 30° intervals from 0° to 180°). For example, a clast with an azimuth of 35° from the dip direction was classified in the interval from 30° to 60°. We did not directly measure the inclination (plunge) angle of their long axis; instead, we roughly categorized clasts into two groups: clasts inclined within 45° of the surface (for which we recorded azimuth, as described above) and clasts that were more steeply inclined (for which we did not record azimuth, and placed them into their own category, see Fig. 14). While this rough method does not yield precise clast azimuth and plunge, it does allow us to compare whether clasts favored a certain organization. To ensure a representative sample, we drew at least 95 clasts at each site. Clasts lacking a clear orientation because they were too spherical (with a long axis less than twice the length of the short axis) were counted separately and did not count towards the minimum sample size.

3.6. Deposit contact

Outcrop C-2 (Fig. 2) additionally allowed us to investigate the contact between the detachment deposit and the underlying hillslope. We cleaned the outcrop using a metal blade and a thin section sample was taken (at the contact) using a putty knife and a plastic beaker. The sample was impregnated with resin, dried, cut, and subsequently polished in the thin section laboratory of Thomas Beckmann, Germany following Stoops (2020).

4. Results

Our field investigations were conducted on the deposits after all the detachments had occurred, while the remote-sensing observations document the emplacement and post-deposition evolution of the deposits. In the following, we focus on distinctive features that may either be unique to glacier detachment deposits or help to distinguish these deposits from those left by rock avalanches, debris flows, or surging glaciers.

4.1. Flat Creek

4.1.1. Remote sensing analysis: landscape impacts of glacier detachments (2013–2016)

The mass flow from the 5 August 2013 detachment started at an elevation of 2200 m asl and traveled down to 1140 m asl, covering a distance of 10.8 km (H/L = 0.11 or an angle of reach of 6°). On its journey, it eroded the original river channel for about 1500 m before depositing large amounts of debris and ice along the river, as well as on top of an 80 m tall hill on the west side of the channel (labeled West Hill in Fig. 2). On the alluvial fan, the flow veered west before turning north towards the White River, leaving behind a long, skinny deposit with thicknesses of 10 m to 20 m (Fig. 2). At the transition between the channelized reach and the alluvial fan, a long levee up to 27 m thick was deposited (henceforth the "2013 levee", see Fig. 2). The 2013 deposit was photographed by Bucknell University geologist Jeff Trop on an overflight on 7 July 2015. These photos – the only close-up images of the 2013 deposit (see Appendix A) – show a lumpy deposit that strongly resembles what we later found in the field after the 2015 detachment.

On 31 July 2015, almost exactly two years after the 2013 event, much of the remaining glacier detached. This detachment initiated at an elevation of 2600 m asl and traveled down to 1035 m asl, covering a distance of 12.7 km (H/L = 0.12, or an angle of reach of 7°). Constrained by topography, the flow initially followed the same path – scouring more of the channelized reach – before spreading new and remobilized debris across vast parts of the alluvial fan (Fig. 2).

In the channelized reach, about one third of the way between the cirque and the alluvial fan, satellite imagery shows several flow-parallel lineations on the northern side of the channel (Fig. 3). We adopt the term

"debris stripes", following Kääb et al. (2021), to describe these lineations visible in the runout path of glacier detachments. In our case, the stripes are on the outside of the first banked turn made by the 2015 mass flow (the 2013 flow did not bank as high on this slope), which scoured the hillslope by up to 2 m. They extend for about 700 m on the slope that is roughly 30° steep. As of 2009, the hillslope was covered by loose regolith and dotted with sparse vegetation, which was removed by the glacier detachments, confirming the scour. We therefore believe that the debris stripes are likely erosional features, though we cannot rule out the possibility that they are depositional features on top of a scoured surface.

Once on the alluvial fan, the 2015 flow overran the 2013 levee. A series of flowbands whose shape resembles the shape of the 2013 deposit are evidence of the shear experienced by the flow as it overran the 2013 levee. Beyond the 2013 levee, the flow split into different branches that protrude into the surrounding forest (Fig. 2). Most of these branches appear to have at least partly followed old drainage channels with sparser vegetation, although vast areas with healthy forest stands were also overrun. Piles of trees and transverse ridges terminate the branches' distal ends. In many places the deposits are bordered by long levees along the sides. Between the levees we found densely-packed, meter-scale and mostly conical mounds of debris (Fig. 4). Among the flowbands and debris mounds, clusters of water pockets, meters to tens-of-meters in diameter, dot the deposit surface (Fig. 4). These water bodies are clustered along the main runout path, where we expect larger ice blocks to be deposited as the mass flow decelerated on the fan. For this reason, we interpret them as indicators of melting glacier ice (Fig. 2).

The 2015 detachment eroded and deposited 5 m to 15 m of material; it is this surface that we were primarily able to access in the field. Cumulatively, the 2013 and 2015 events removed 30 m to 100 m of ice and lithic material from the glacierized cirque and left 2 m to 30 m thick deposits in the channelized reach and on the alluvial fan. The thickest deposits are found on either side of the river just upstream and downstream of West Hill, as well as on the alluvial fan (Fig. 5a).

On 16 August 2016, part of neighboring glacier 01.22616 (RGI-ID, RGI Consortium (2017); Fig. 2) also detached. Between 2012 and 2016 the upper part of the glacier thinned while the lower part thickened (Fig. 5a). The detached tongue was around 30 m thick and covered an area of about 0.14km^2 (Fig. 5b; details reported in (Kääb et al., 2021)). Good quality, timely satellite images are lacking for this period, but a video captured by park rangers on a coincidental overflight shows that the icy flow remained largely confined to the bottom of the channel, though it did bank high over previous deposits near the source (see https: //youtu.be/Xh23H3QApk8). While the 2013 and 2015 flows deposited large amounts of debris, the 2016 event consisted of water and ice with a very low sediment content. Satellite imagery acquired in the years after the 2016 event show no visible traces of this event.

4.1.2. Remote sensing analysis: post-detachment landscape response (2016–2019)

The post-detachment landscape response takes many forms. Below, we review the changes visible in the DEMs and orthophotos, moving downstream from the glacierized cirque, to the channelized reach and the alluvial fan.

In the cirque, between 2016 and 2019, remnant glacier ice flowed into the emptied trough and lead to a mean surface elevation increase of 17.7 m (maximum of 50 m; Figs. 5b and 6). As a consequence, the remaining glacier thinned by an average of 9.2 m and a maximum of 37 m. This debuttressing response left the glacier heavily fractured and pulled ice away from the ridgeline, leading to increased rockfall activity and debris accumulation in the release zone.

Immediately downstream of the detachment zone, a large wedge of ice and debris – 10 m to 20 m thick in 2016 (relative to the 2012 surface) – is steadily being eroded by a network of streams. Changes in this uppermost part of the channel are large, and the dynamic nature of the landscape make it hard to interpret all of the elevation changes. The erosion of the ice wedge and other deposits lining the channel has led to widespread aggradation, raising the river bed by up to 8.5 m between 2016 and 2019 (Fig. 5). Alongside the active channel, many of the deposits thinned significantly as the ice within them – confirmed by the ERT measurements (Section 4.1.4) – melted (Fig. 6a). These downwasting signatures often manifest in an elevation decrease that is larger and more confined than that of its immediate surroundings. The elevation change maps also show material eroding from the steeper sections of the drainage and accumulating closer to the river, where it leads to an elevation increase, immediately downslope of a height decrease. Across all the ice-rich deposits, the surface lowering is generally around 1 m to 2 m (0.3myr^{-1} to 0.6myr^{-1}) between 2016 and 2019, though values can be as high as 10 m locally.

The alluvial fan underwent numerous changes between 2016 and 2019 – changes which can help us understand how such a deposit will likely evolve in the future. The largest changes here remain in the area directly impacted by Flat Creek, with meter-scale aggradation and bank erosion. However, the elevation changes show that the material remobilized by the river largely has not (yet) reached the White River. Instead, our results suggest that in raising its own bed, the river was able to breach a levee and start flowing north, following a more direct course towards the White River. This has led to a patchwork of erosional and depositional regions in the new drainage path of Flat Creek (Fig. 7). With more space to move, the river is widening and progressively eroding the meters-thick deposits along its flanks, gradually destroying the evidence of past events. This has also led to some undercutting of the banks on the eastern side of the river. Here, however, the initial deposits were thin, and we primarily detect a signature of surface raveling on the steeper banks right above the river.

Outside the areas where the river has deposited remobilized

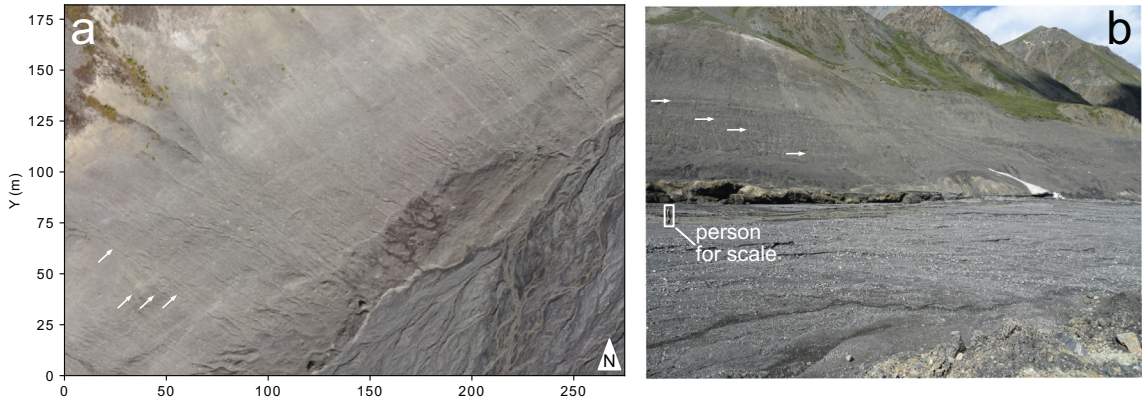

Fig. 3. Debris stripes visible in (a) vertical and (b) ground-based photos. The white arrows indicate the directions and start of stripes left by the 2015 mass flow; the slope of the hillside is 30°. The x and y axes of a are in meters from the bottom left corner of the box plotted in Fig. 2.

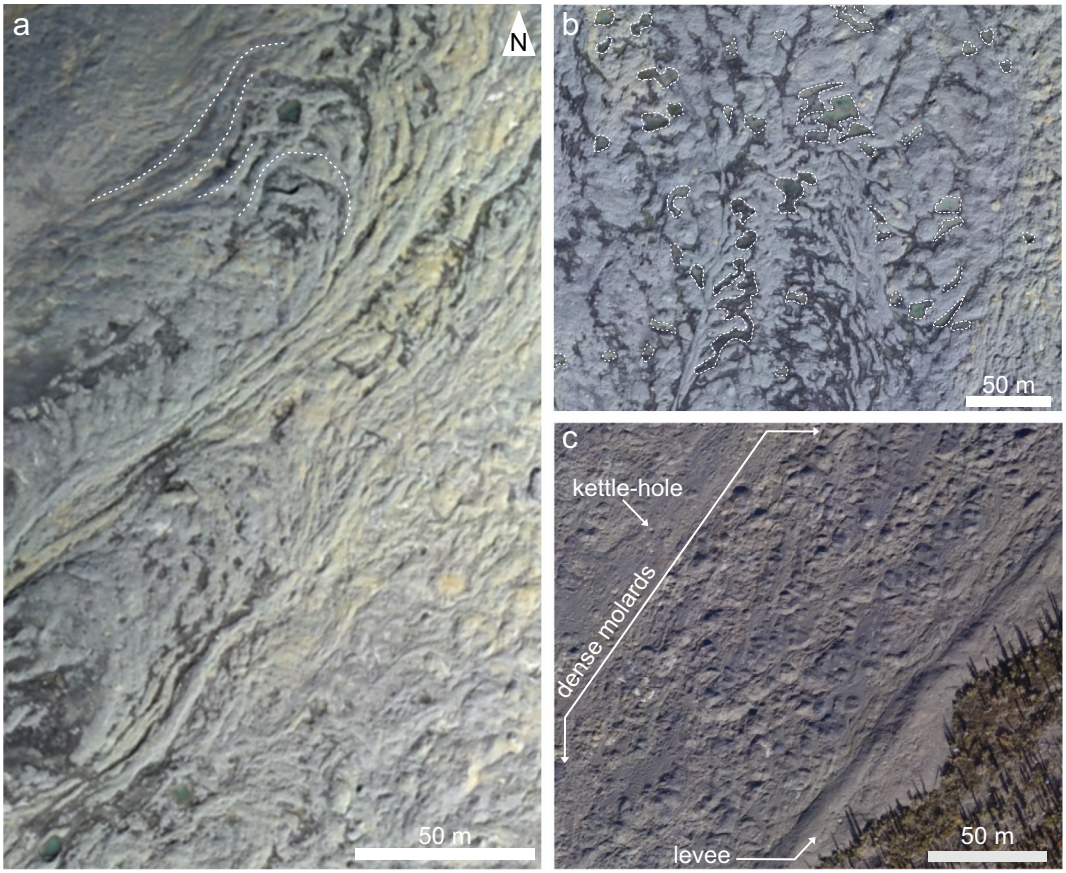

Fig. 4. Birds-eye view of flowbands (a), water bodies (b) and a lateral levee bordering a dense molard field (c) visible in the 2016-06-01 SfM orthophoto. A few flowbands and the largest water bodies are indicated with dashed lines. The image extents correspond to the boxes plotted in Fig. 2.

material, the surface elevation of the deposit has decreased, the clear sign of deposit compaction and downwasting (on the order of dm). We interpret any surface increase in areas far from the river as residual errors from the DEM processing. However, the pattern of surface lowering is not even across the fan: Some of the largest values can be seen in the area where the 2013 levee was deposited. Here, meter scale thinning, likely caused by the melting of large, buried ice bodies (Fig. 8), is visible. This thinning is larger than the compaction of the neighboring ice-poor areas, leading to the formation of large tension cracks. We initially mapped the most ponds in this same region, almost all of which have since drained, leaving behind a pattern of shallow craters that is clearly visible in the elevation change map (Fig. 7).

4.1.3. *Field observations*

The Hasen Creek sedimentary rocks that make up the Flat Creek cirque consist predominantly of thin-bedded layers of dark grey and tan to reddish brown sandstones and siltstones that disintegrate easily and accumulate in thick layers in and on the cirque's glaciers (Fig. 9a). We were not able to access the release zone to determine a representative stratigraphy of this area due to rock- and icefall hazards. However, the detachment deposit consists almost exclusively of the same siltstones and sandstones that we observed (from a distance) in the cirque. In a few locations we found the same dark grey and tan colors present as distinct layers of fine-grained debris in the deposit, suggesting that, in some cases, there was limited mixing of the original materials during transport (Fig. 9b). We were not able to find any evidence that these layers represented preservation of an existing source stratigraphy, nor did we find sections of intact bedrock that would have retained an original source stratigraphy (Fig. 9a).

With the exception of a handful of boulders, the ice-free parts of the detachment deposit are mostly composed of angular to subangular clasts surrounded by a fine-grained, clay-rich matrix. The high clay content causes the deposit to become very soft when wet and hard as concrete when dry. We did not observe any vertical or horizontal sorting.

Occasional boulders from the Hasen Creek formation imply that some highly incompetent bedrock was included in the detachment and subsequent mass flow. Occasional boulders of the Nikolai Greenstone formation, derived from bedrock downstream of the detachment zone, indicate that bedrock was also entrained by the mass flows following the release.

We found large, conical piles of debris throughout the deposit. Termed molards, these piles are common features on periglacial mass-wasting deposits, although they are not exclusive to these, and have been linked to the post-depositional degradation of ice-cemented blocks (e.g., Brideau et al., 2009; Milana, 2016; Morino et al., 2019). Some molards are very distinctive, standing alone and composed of a lithology that contrasts their surroundings (e.g., a tan pile on a grey surface, see Fig. 9d). Across vast parts of the deposit, however, the surface is bumpy and individual molards are harder to pick out, suggesting that here, countless closely-spaced molards are superimposed.

We also found several peculiar clasts firmly embedded in deposited debris and superficially scratched in the direction of the flow (Fig. 9c). These clasts were all cobble size (10 cm to 20 cm in diameter), easily small enough to be entrained by the flow. They were exclusively found on the leeward side of a hill over which the mass flows had passed (see location in Fig. 2).

We investigated the contact between the deposit and the underlying hillslopes in one location (near C-2 in Fig. 2). Here, near the upper edge of a banked turn, there was hardly any mixing of the debris with the underlying hillslope (Fig. 11). We did not find traces of vegetation between the two layers, suggesting that it must have been removed – likely with the uppermost soil horizon(s) – before the new material was deposited.

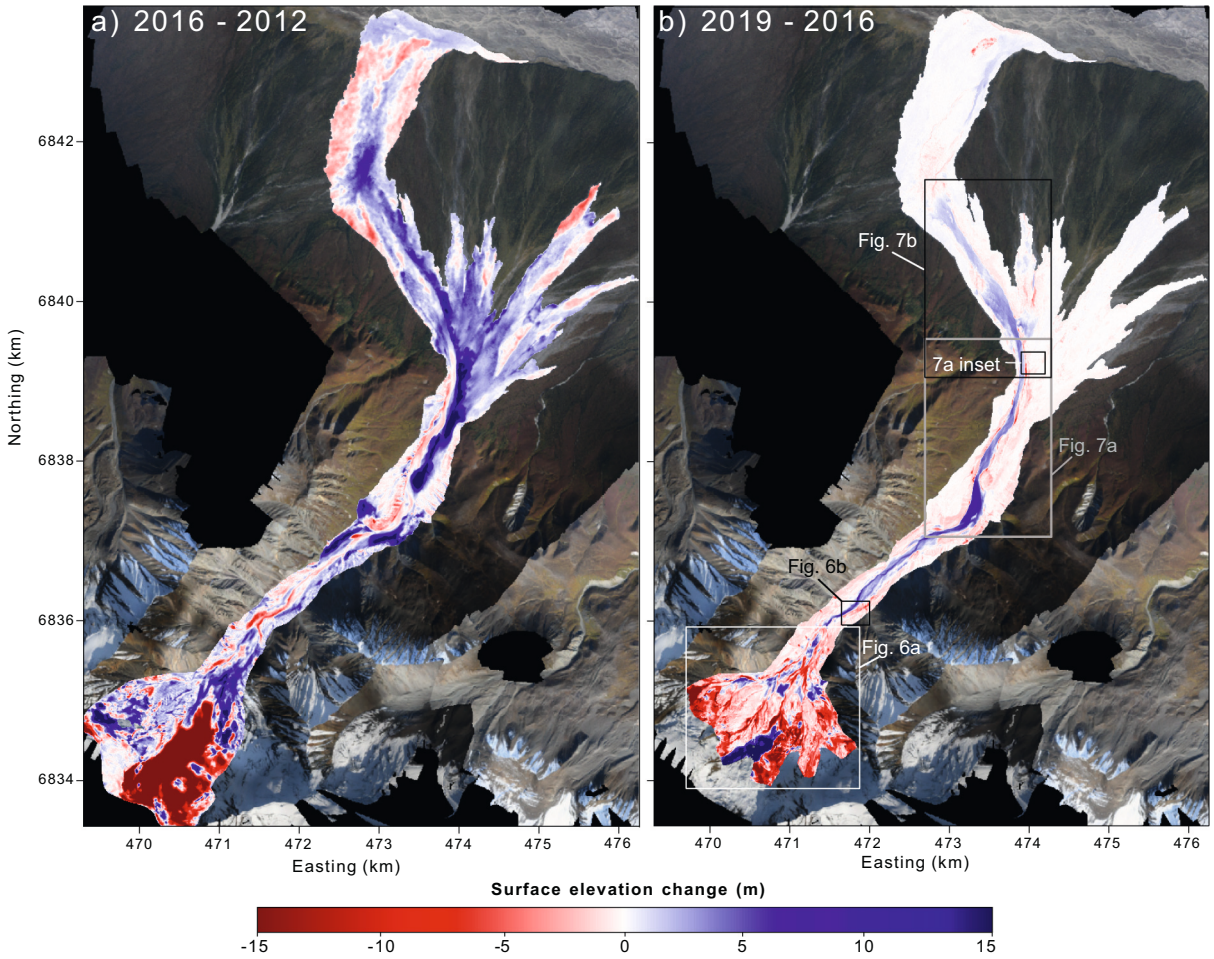

Fig. 5. Cumulative surface elevation changes (a) between 2012 (AK IFSAR) and 2016 (ArcticDEM), including changes from the 2013 and 2015 detachments and (b) between 2016 and 2019 (both SfM DEMs), including changes from the 2016 detachment. Negative values indicate surface lowering.

Finally, the fate of the detached glacier was evident in large outcrops of ice conglomerates; rounded ice blocks, cemented together by a matrix of muddy ice. The blocks of clean glacier ice were cobble to boulder sized, and the matrix that held them together appeared to be made of ice that had disintegrated during transport and reconsolidated upon deposition (Fig. 10a). These ice conglomerates were visible for tens of meters along the river channel – sometimes only covered by a thin veil of debris (Fig. 10c/d) – and we found them up to ~6 km from the release zone (as of 2018/2019). Even where ice was not directly visible, soft, water-saturated sediments and tension cracks in the overlying sediment often indicated the presence of residual melting ice (Fig. 8). On the alluvial fan, we found numerous kettle holes across the deposit. In some cases – even in 2019, four to six years after the detachments – we still found freshly-collapsed, straight-walled holes that indicated continued and active degradation of buried ice blocks.

4.1.4. Electrical resistivity tomography

The electrical resistivity surveys confirmed that much of the observed downwasting and settling of the deposits can be attributed to ice melt. Of the eight electrical resistivity surveys conducted on the Flat Creek detachment deposits, three showed large bodies of resistive material which we interpret as ice (lines 5, 6, and 8 – see Fig. 12). These results show that in many places, the deposit still contains ice bodies that are 10 m to 20 m thick. The measured values around 10,000 Ωm are low for solid ice (typically 100 kΩm to 1000 kΩm; Kneisel et al., 2008), but very plausible for fragmented, debris-rich, actively-melting ice. Although we did not see ice at the surface of any of these transects, nearby ice outcrops, sagging wet ground, and fresh tension cracks support our interpretation. Furthermore, the suspected ice bodies in profiles 5, 6, and 8 are within bodies of lower-resistivity material (< ~1000 Ωm), which eliminates the possibility that they may be dry bedrock outcrops (which would also show up as highly resistive). All three lines show highly conductive areas directly below the suspected ice, which we interpret as accumulating meltwater.

Conversely, line 4 (Fig. 12) confirms that the thick, wet, but ice-free (or ice poor) deposits have a much lower electrical resistivity (Fig. 2). Line 4 is representative of the other transects that lacked a presence of large ice bodies (see Appendix B). These ice-free locations were all at a greater distance to the main channel, or in one case, directly in the river channel, where any ice would have been eroded or melted by the river. In other words, the ERT measurements confirm that large ice bodies are present in the detachment deposit along the central flowline of the mass flows (which largely correspond to the active river channel), but not elsewhere.

4.1.5. Grain size analysis

The grain size distribution of the Flat Creek detachment deposit differed markedly from that of its surroundings. The samples from the detachment deposit (samples 1–7, in order of increasing distance from the release zone) contained more fines (< 1 mm) and fewer large clasts (~15 % vs. 65 % clasts >20 mm) than the other samples (Fig. 13). The samples from the river channel were a testament to the power of the water: originally from the same detachment deposit, these two samples lost a significant part of their fines and attained grain size distributions closely resembling those of the hillslope samples. The hillslope samples, in turn, contained lower amounts of fines and more large clasts than the

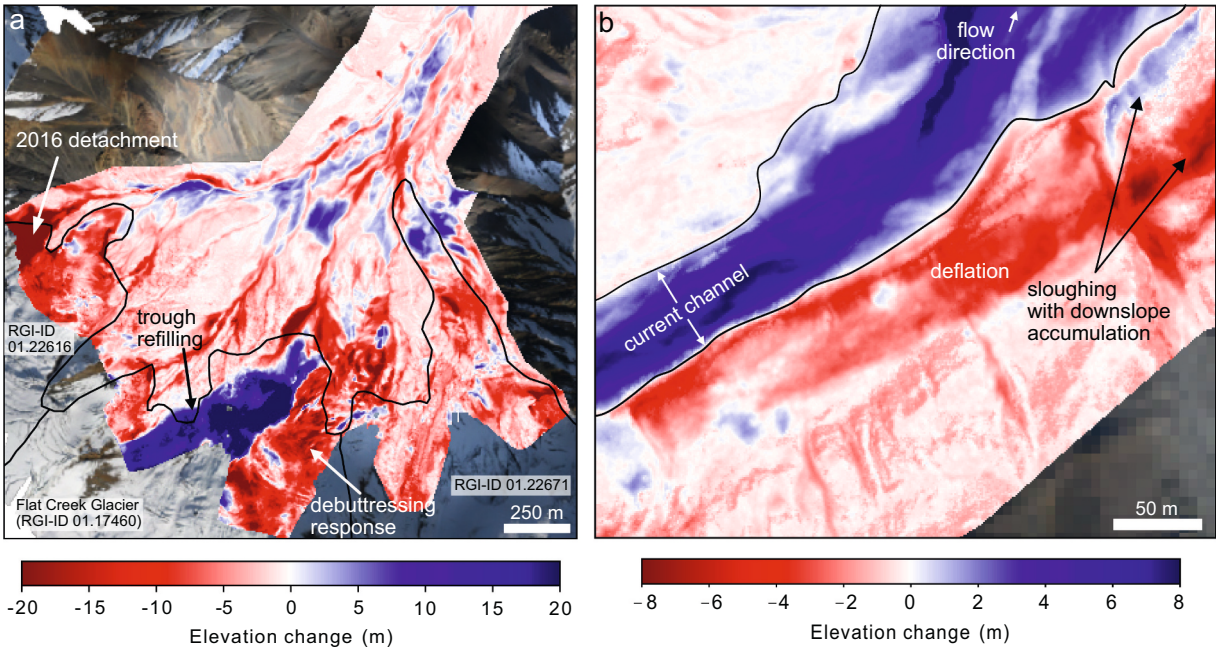

Fig. 6. (a) Post-detachment landscape response in the glacierized cirque between 2016 and 2019 (both SfM DEMs). The refilling of the trough from which the detachment originated has led to substantial thinning on the remaining glacier. The black lines are the original glacier outlines from the Randolph Glacier Inventory (RGI). (b) Levee downwasting and sloughing in response to the melting of buried ice (ERT line 5 was measured at this location – see Figs. 2 and 12) and river erosion.

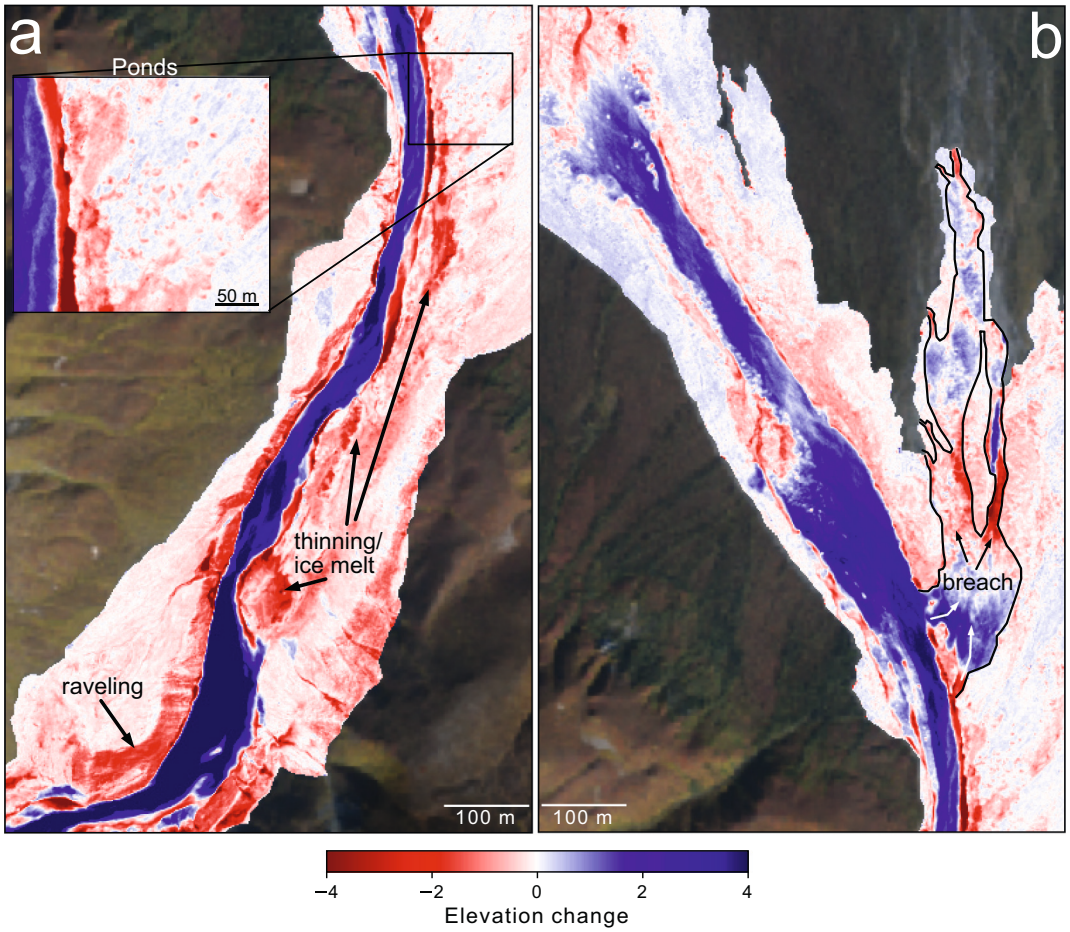

Fig. 7. Elevation changes in the lower channelized reach (a) and central fan (b) where we see a major breach in the lateral levee, widespread thinning, raveling, and the pockmarked appearance of the deposit where thermokarst ponds appear.

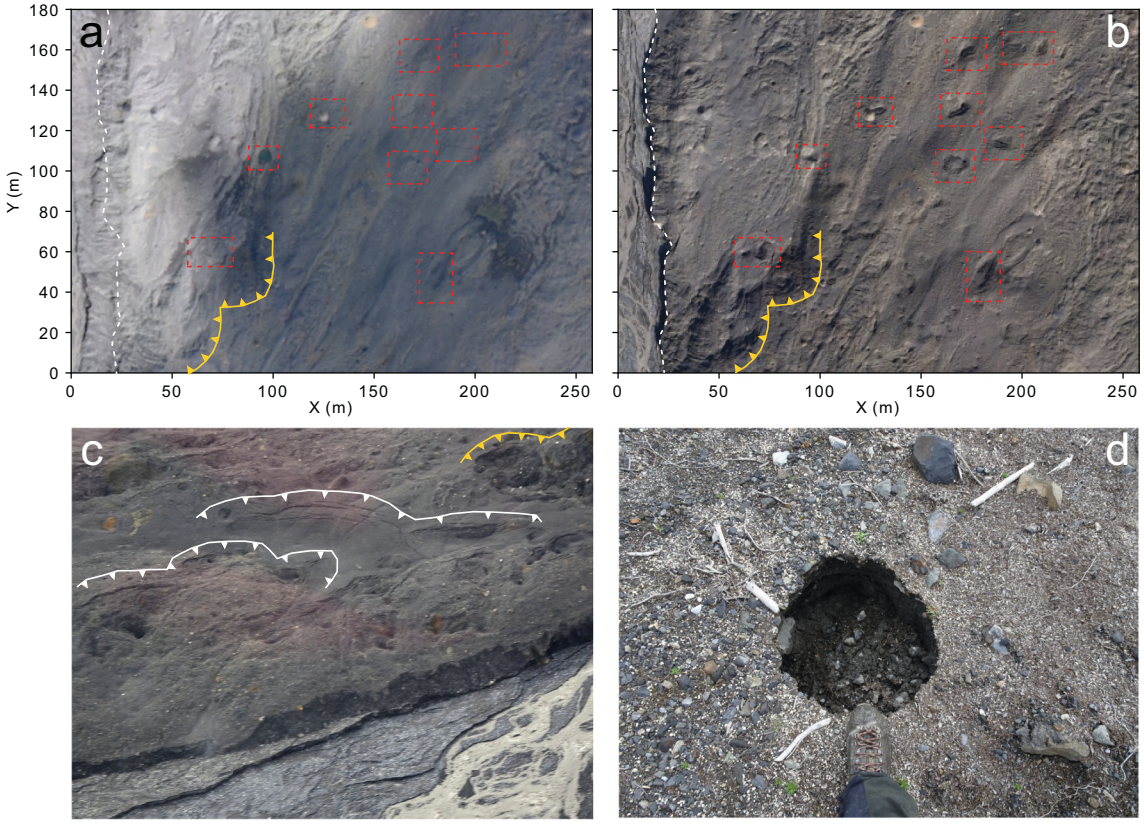

Fig. 8. Aerial views of a region of the deposit with widespread thinning, as seen in 2016 (a) and 2019 (b) orthophotos and (c) from a helicopter in 2020. Dashed red boxes indicate areas that deflated between 2016 and 2019, yellow and white lines mark the edges of large scale downwasting (arrows pointing downhill). Melting of small ice-blocks leaves meter-scale, straight-sided circular kettle-holes (d). The x and y axes of (a) and (b) are in meters from the bottom left corner of the boxes plotted in Fig. 2.

samples from the detachment deposit. They also spanned a very wide range, especially between 0.5 mm and 50 mm, where they bracket the river samples.

In addition to the individual grain size distributions, we analyzed the spatial relationships between the samples. The lines in Fig. 13 are color coded to visualize the increasing distance from the release zone (dark red = proximal, light yellow = distal; compare Fig. 2). We did not detect any sorting in the deposits, whether with increasing distance from the release zone, nor with increasing distance from the center of the channel. Spatial proximity of sampling locations did not predict similarity. Samples 1 and 2, although collected from the same pit (but from layers of debris that differed in color: dark grey vs. tan), are surprisingly different. In contrast, samples 6 and 7 were taken about 50 m apart and yielded very similar results (no layering was present here).

4.1.6. Clast orientations

Clast orientations in the detachment deposits were starkly different from those in the underlying hillslope (Fig. 14). The clasts extracted from the detachment deposits were generally pebble-sized and angular. At C-1, the surface of the deposit – presumably aligned with the flow direction – dipped NE. Clasts had a slight preference for pointing N, in approximate alignment with the flow direction, but were roughly evenly divided between the two inclination categories (48/114, or 42 %, were steeply inclined). Similarly, clasts in the detachment deposit at C-2 had no preferred heading or inclination (41/112, or 37 %, were steeply inclined). In contrast, the long axes of the hillslope clasts at C-2 preferentially pointed WNW, in the dip direction of the hillslope, and almost all were clearly inclined along the surface dip (Fig. 14). These clasts were significantly less angular, pebble to cobble sized, and many had thin layers of clay on their surface.

4.2. East Site

In addition to recording observations from a known glacier detachment deposit at Flat Creek, we compared its characteristics with observations from a nearby deposit that is at least superficially similar to Flat Creek and predates the satellite record. The East Site deposit and the glacier upstream of it are visible in a 1978 aerial image (Alaska High Altitude Photography; AHAP) and appear almost unchanged compared to today. Whatever the origin of the deposit, it must have been emplaced by the mid twentieth century. For this reason, we decided to apply our land-system model to a deposit below a glacier with a similar climate and geometry – two possible factors impacting the likelihood of a glacier detachment.

4.2.1. Deposit morphology and evolution

The glacier in the East Site drainage (RGI60-01.17534) covers an area of just under 1.5km^2 between 1915 m and 2580 m asl, has a mean slope of 19°, and currently terminates about 600 m upstream of the old deposit. The terminus of the crevasse-free tongue in modern imagery appears stable relative to its position in the 1978 AHAP image and features several meandering supraglacial streams. Crevasses are absent on the glacier with exception of a bulging step about halfway up the glacier.

The deposit is about 1.3 km long and is sparsely vegetated. No lake is visible in the AHAP images, but Landsat imagery indicates that a lake first appeared in the late 1990s. DEM differencing of the 2012 and 2016 DEM shows that the depression holding the lake continued to expand (from roughly 20 000 m^2 to 26 000 m^2), primarily by retrogressive erosion of the banks. A comparison of the 2009 Ikonos image, the 2019 orthomosaic, Planet and Google Earth images revealed that the lake area

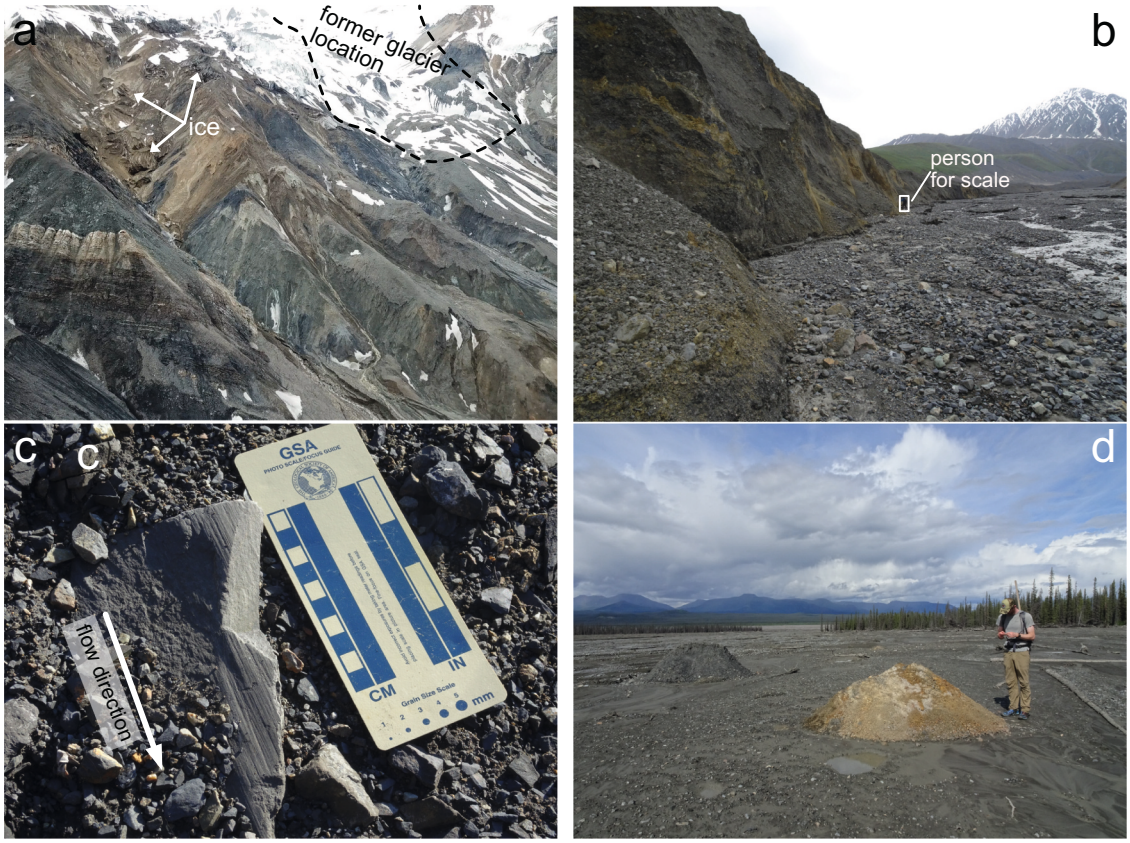

Fig. 9. Photographs of the release zone and the deposits. a: Release zone surrounded by the typical dark grey and tan siltstones and sandstones. b: Thick deposits left by the mass flows along the channel just beyond the fan apex, with dark and tan layers of debris visible as distinct layers. c: One of the striated rocks found on the leeward side of a small hill in the upper part of the catchment. d: Two isolated molards near the confluence with the White River, again showing the two distinct rock colors.

regularly fluctuates between about 500 m^2 and 12 000 m^2. On the south-eastern side of the lake, the deposit exhibits a particularly striking rock glacier-like ridge-and-furrow structure (Martin and Whalley, 1987) that is around 400 m long and 100 m wide. Manual feature tracking (2009 Ikonos vs. 2019 Sfm) reveals displacements of around 1myr^{-1} of this part of the deposit, suggesting gravity-driven creep.

4.2.2. Field observations

The morphology of the East site deposit is strikingly different than that of the deposits at Flat Creek. The surface is covered with larger clasts, which we interpret to be a consequence of the local geology: the East Site lies fully in the Nikolai Greenstone formation (Fig. 1), where the more resistant basalts erode less easily than the thinly-bedded sedimentary rocks found in the Hasen Creek formation. The transverse ridges and furrows terminate in steep lobes at the edge of steeper terrain. We did not find the widespread molards or hummocky terrain that we found at Flat Creek (Fig. 15b), and the surface is generally firm and easy to walk across.

At the center of the deposit, there is a large block of ice partly buried under debris but exposed and accessible from the shore of the small lake. This ice lies at the most distal end of the part of the deposit that exhibited visible surface displacements. We found the ice to be intact and contain the typical horizontal layers found in glaciers as a result of seasonal accumulation and melt (Fig. 15c/d). These layers were parallel to each other, suggesting that the ice had not been substantially displaced, broken up or rotated.

4.2.3. Electrical resistivity tomography

The ERT surveys confirmed that the large body of intact ice extended below the debris. Line 10 (Fig. 16) had resistivities more than five times higher than the highest observed in other lines, indicating that a block of solid ice tens of meters thick lies beneath about 5 m of highly conductive sediment. The location of this block at the distal end of the area that exhibits creep suggests that ice-rich conditions are likely present in this area of the deposit. Lines 11 and 13 (Fig. 16) show electrical resistivity values that are similar (or locally higher) to what we measured on ice-rich transects at Flat Creek. However, the surface of the deposit was dry, with no tension cracks, kettle holes or ponding. Because electric current is primarily transmitted via liquid water, dry ground or debris with large air pockets is generally highly resistive to electrical current (Kneisel et al., 2008). In contrast to the ice-rich deposits at Flat Creek, where electrically resistive areas were surrounded by highly conductive material, the electric resistivity here is high throughout (>10 kΩ). We therefore interpret that these results indicate not the presence but rather the absence of ice, and conclude that the deposit north-west of the lake is largely ice-free.

4.2.4. Grain size analysis

We analyzed the grain size distributions of three locations at the East Site (Figs. 2 and 15a). Samples 8 and 9 were collected close to the lake, in proximity to the ice, and sample 10 came from a more distal part of the deposit at the front of a steep lobe. Fig. 17 shows the grain size distributions of these samples plotted against the envelope of the samples that were collected from undisturbed parts of the detachment deposit at Flat Creek. Sample 8 – collected right above where the ERT measurements showed a large block of ice – falls fully within the envelope of the detachment samples from Flat Creek. Sample 9 is similar, but lacks the very small fraction and is enriched in larger clasts. Sample 10 is distinctly different from the detachment samples. Due to the limited number of samples we were able to collect at this site, we cannot

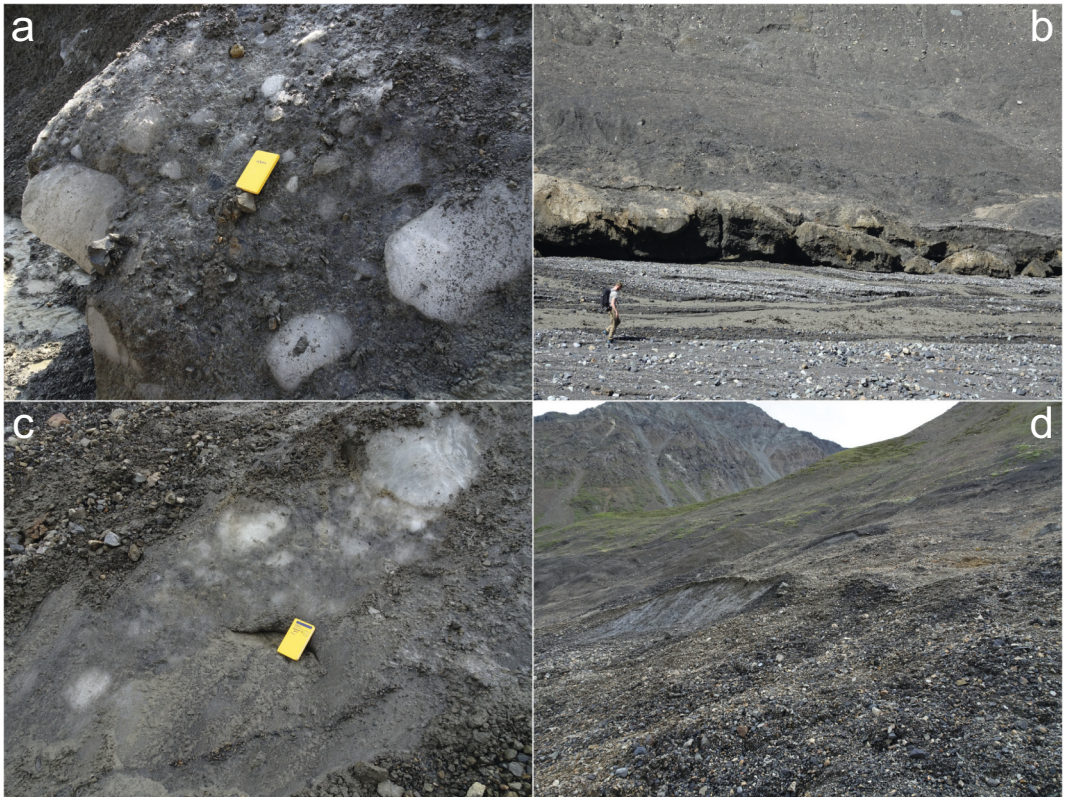

Fig. 10. Relic glacier ice in the detachment deposits at the Flat Creek Site. (a) Rounded blocks of ice and small rock clasts cemented together in a matrix of muddy ice along the river channel. (b) Large blocks of debris-rich ice or reconsolidated ice undercut by, and toppling into, the river. (c) + (d) Large bodies of solid ice visible as retrogressive thaw scarps under a thin veil of debris.

Fig. 11. (a) Contact between the original hillslope (bottom, brown) and the detachment deposit (top, dark grey) near where we measured clast orientations. (b) Sample extracted in the vicinity of the outcrop in (a). The contact shows very little mixing between the two layers.

draw any conclusions about spatial patterns in the grain size distributions, nor were we able to determine whether any of the three samples is representative of the larger deposit.

5. Discussion

The Flat Creek Glacier detachments had a profound impact on the landscape that will likely be visible for decades or centuries. But can the morphology and makeup of these evolving deposits help us identify the traces of such catastrophic events in the geologic record, and can we distinguish them from other mass-movement deposits? Here, we evaluate the significance of our findings for identifying glacier detachment deposits, compare them to deposits of rock avalanches, debris flows and glacier surges, and use these findings to assess the history of the East Site deposit.

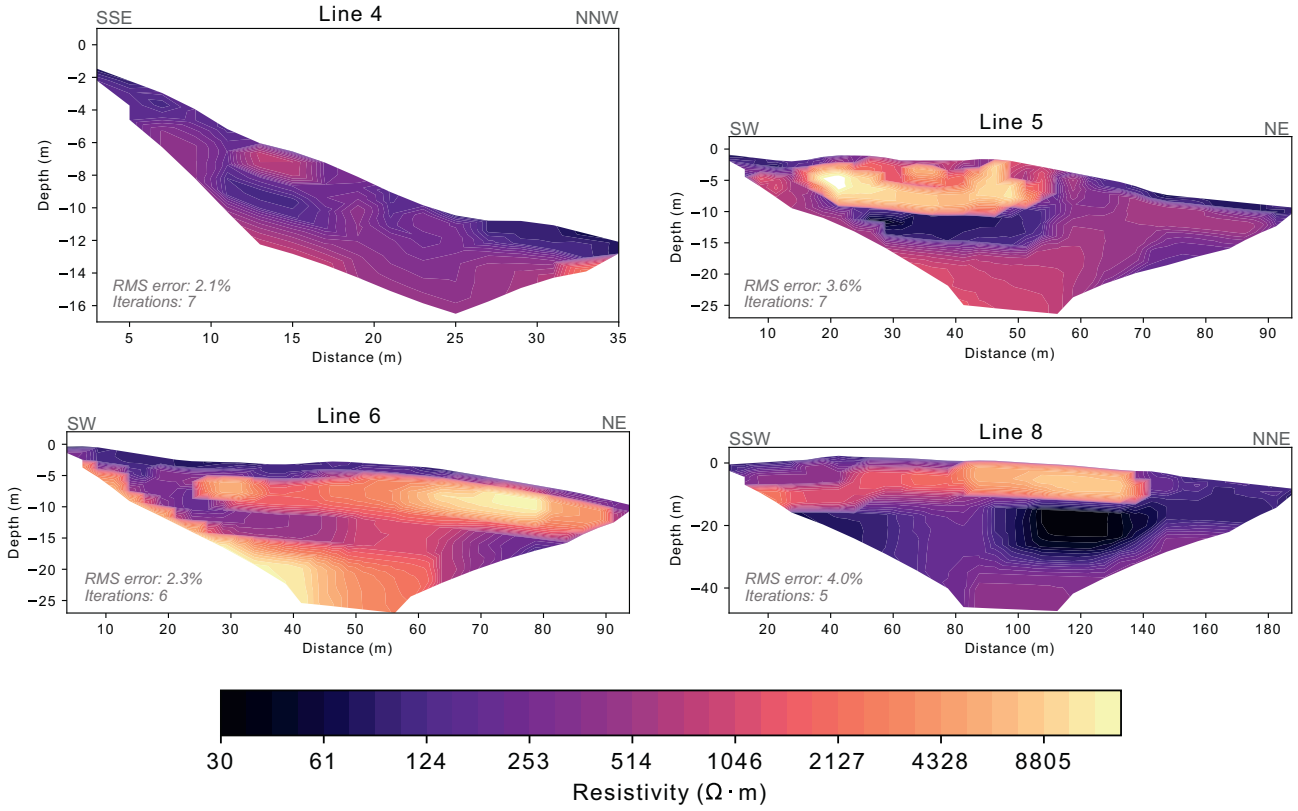

Fig. 12. Electrical resistivity survey lines 4–6 and 8 on the Flat Creek deposit. The color scale is logarithmic; light colors indicate high resistivity to electric current, dark colors indicate low resistivity. Line 4 is representative of ice-free profiles on the deposit. Transects 5,6, and 8 ran parallel to the river, transect 4 is at a distance and further uphill.

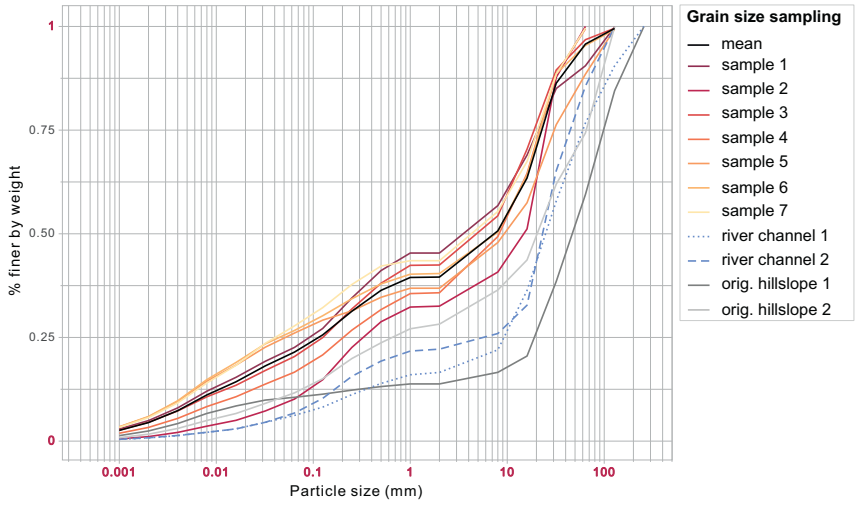

Fig. 13. Grain size distributions of the Flat Creek detachment deposit, compared to those of the original hillslope and the active river channel. The detachment samples 1–7 are color coded to visualize the increasing distance from the release zone (dark red = proximal, light yellow = distal; compare Fig. 2).

5.1. Depositional signatures of glacier detachments

One of the challenges of interpreting the Flat Creek deposits is that they were the result of three separate detachments; and we could not always determine the specific history of a sampling site. The 2015 detachment had the greatest impact on the landscape, but it is possible that we also sampled from the 2013 or 2016 detachments. However, we believe that treating all the events as one is justified due to their similar nature and the fact that other deposits in the geologic record may also be the result of multiple detachments.

Below, we discuss the different features of the deposits, sorted by their presumed longevity – from the most ephemeral to the most persistent.

5.1.1. Ice and icy deposits

Large amounts of glacier ice were still present in the deposits in 2018 and 2019. Rounded blocks of ice, compacted into large debris-rich ice bodies, are evidence of the violent nature of glacier detachments. These ice-rich deposits are also the least persistent feature: based on our estimated melt rates of 0.3 myr^{-1} to 0.6 myr^{-1}, the 10 m to 20 m thick ice

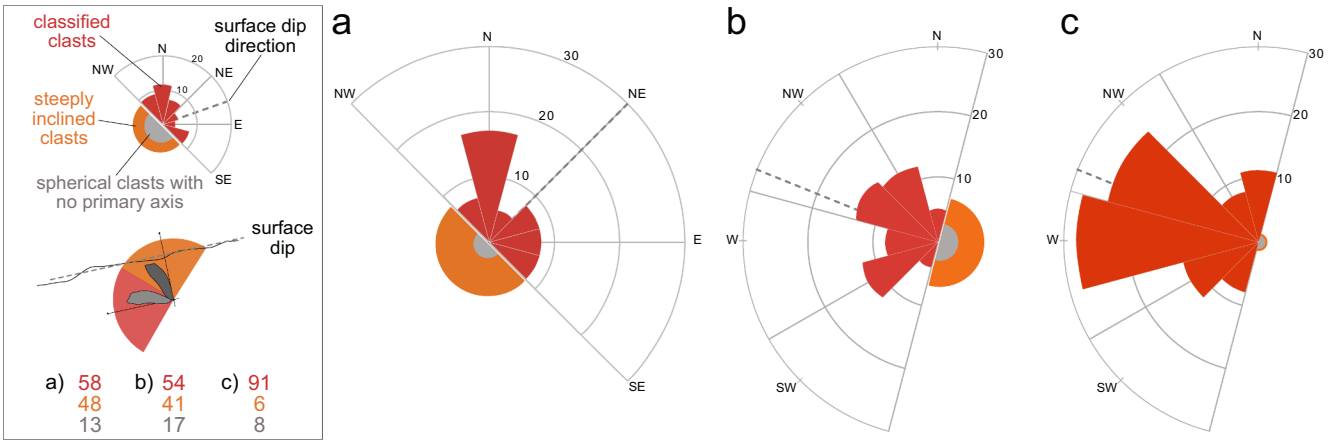

Fig. 14. Clast orientations measured at two outcrops: (a) C-1 detachment deposit, (b) C-2 detachment deposit (c) C-2 original hillslope (Fig. 2). The heading of the petals indicates the azimuth of the clasts; the length of the petals indicates the number of clasts with that heading. The dashed line indicates dip direction of the local surface. The orange area represents the number of steeply inclined clasts (> 45° plunge), the grey area represents the number of clasts that lacked a clear long axis. The individual numbers are given on the left.

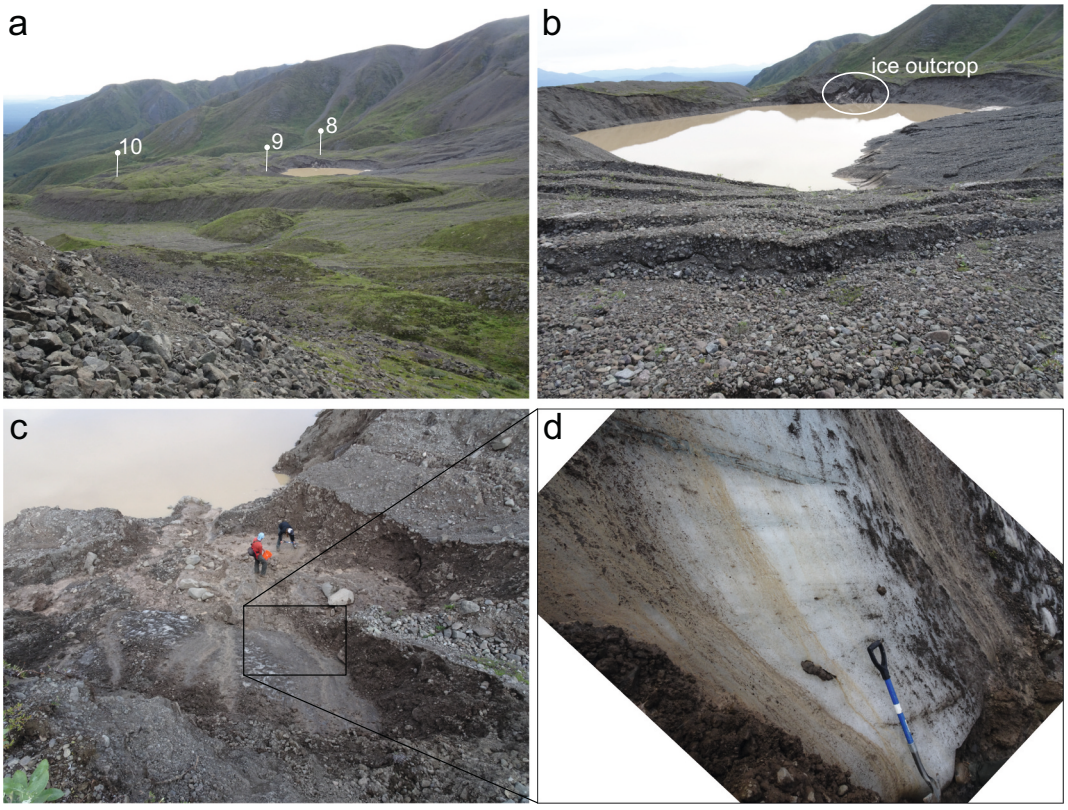

Fig. 15. Overview of the East Site. a: Photograph of the lobate deposit with the lake at the center and the locations of the grain size samples pinpointed. b: Lake with exposed ice on the far shore (circled). c + d: View down onto the exposed ice and a section of the ice showing the typical parallel layers found in glacier ice.

layers will disappear in 15 yr to 60 yr. These melt rates are somewhat higher than those reported for dead ice deposits (Driscoll, 1980; Krüger and Kjær, 2000; Schomacker and Kjær, 2007, 2008), likely due to the fragmented and debris-rich nature of the ice in the detachment deposits. Glacier detachment deposits that predate the satellite era are thus likely to contain little to no ice, lending greater importance to the interpretation of geomorphic and sedimentary features.

Where the ice-rich deposits are in direct contact with the river, fluvio-thermal erosion is leading to a rapid and complete removal of the deposits. Further from the river, distinctive thermokarst features can persist for longer. Sharp-edged tension cracks diffuse over time, but differential settling patterns remain visible. Likewise, the straight-edged kettle holes transform into conical depressions in no more than one or two years, but are likely to persist for much longer in this stable geometry. Most are only a few meters in diameter and less than one meter deep, so high-resolution data would be necessary to detect them, although some may persist more visibly as small ponds. The largest depressions were clustered along the river, but many of them disappeared when the river straightened its course in 2019 (Fig. 2). Eventually, the regrowth of vegetation will make identification of these surface features increasingly difficult.

A missing, or unusually small, glacier can indicate a past glacier

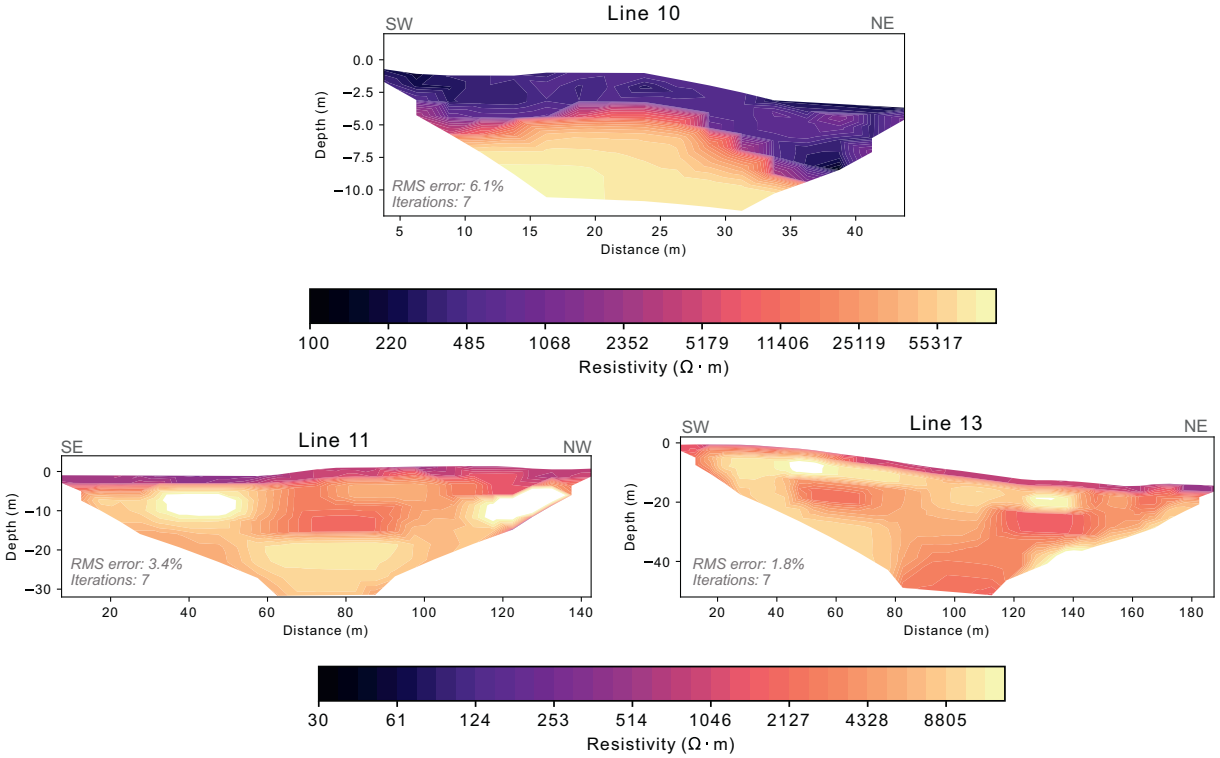

Fig. 16. Results from electrical resistivity survey lines 10, 11, and 13 on the East Site deposit. The color scale is logarithmic; light colors indicate high resistivity to electric current, dark colors indicate low resistivity. Note that the color scale of the upper panels differs from that of the lower panels by about an order of magnitude. Lines 11 and 13 indicate relatively high electrical resistivities, likely due to very dry conditions. The very high resistivities visible in Line 10 are due to the presence of a block of old but intact glacier ice.

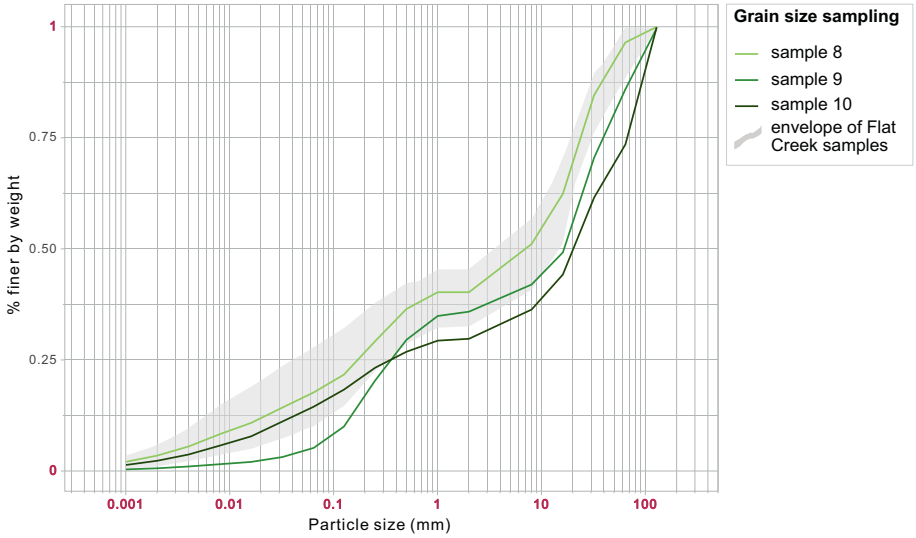

Fig. 17. Grain size distributions measured at the East Site, compared to the envelope of all samples collected from the undisturbed detachment deposit at Flat Creek.

detachment. For example, Kolka Glacier, while slowly regaining mass following its complete detachment in 2002 (Haeberli et al., 2004; Huggel et al., 2005), is still much smaller than neighboring Maili Glacier. However, this difference can be short-lived: at Flat Creek, the remaining ice quickly filled voids left by the glacier detachments. Recent images of the Aru detachment scars show that the side branches of the glaciers, which were not affected by the 2016 detachments (Kääb et al., 2018), are now advancing into the empty troughs. Repeat elevation data can detect this type of compensatory advance, as it invariably leads to thinning of the remaining ice, but such information may not be available for pre-historic detachments.

5.1.2. *Striated clasts and debris stripes*

Striated clasts embedded in deposits close to the release zone may be unique to glacier detachments. Few other glacier detachment deposits have been investigated in detail, but similarly scratched clasts were found close to the detachment zone of Kolka glacier (personal communication Sergey Chernomorets, 2020; and mentioned on https://earthobservatory.nasa.gov/features/Kolka/kolka4.php). Striations in bedrock have long been interpreted as the result of glacial erosion by

sliding, but this implies the motion of an intact glacier (Bennett and Glasser, 2011). We believe it is unlikely that these striae were caused by historical glacier motion because the clasts are embedded in the same fine-grained deposits that make up the rest of the Flat Creek deposits, and several molards also cover the hillside. The mechanism for the creation of these striated clasts by glacier detachments remains unclear. Since they were all found on the leeward side of the hill (labeled S in Fig. 2), perhaps the mass flow became airborne as it came over the hill and these specific rocks, once embedded firmly enough in the deposit not to be moved again, were sandblasted in place.

Similarly, the larger-scale debris stripes may be indicative of a catastrophic glacier detachment. Indeed, Kääb et al. (2021) reported similar lineations in the runout zones of detachments in Tibet, Russia, Chile and Tajikistan. In two cases in the Chilean Andes (Aparejo glacier and Tinguiririca glacier), these stripes were visible in old and new (1960s and today) high-resolution satellite and aerial images, suggesting that they can persist for at least decades. Kääb et al. (2021) stress, however, that more research is needed to determine whether these features can be reliably distinguished from glacier flutes left by past glacier flow (such as those documented in the forefields of glaciers such as Austre and Midtre Lovénbreen on Svalbard; Glasser and Hambrey (2001), Bennett and Glasser (2011)).

At Flat Creek we found the debris stripes exclusively on the outside of the banked turn, where the elevation change map indicates around 2 m of scour by the 2015 mass flow, suggesting that the stripes are primarily an erosional feature. While the origin of the debris stripes documented in Kääb et al. (2021) cannot be determined with certainty, in our case satellite images prove that the stripes were left by the glacier detachments. Additionally, their position on the steep valley flank (slope around 30°) is distinctly different from the flat terrain which typically hosts glacier flutes. Despite these insights, only detailed investigations and broader comparisons can determine how unique such debris stripes are to glacier detachments. Taken together, the parallel lineations – both the striated clasts and the larger debris stripes – also indicate that close to the detachment zone, the flow was not (yet) entirely turbulent.

5.1.3. Molards

The widespread debris mounds were maybe the most notable characteristic of the Flat Creek deposit. They are meter-scale, radially symmetric, and distributed somewhat randomly throughout the deposit – either isolated or superimposed on each other. We have referred to these features as molards because we believe that they largely represent blocks that behaved as solids during transport and disintegrated upon deposition (Morino et al., 2019). In this sense, they are distinct from the hummocks typically found in rock avalanche deposits, which are the consequence of extension and faulting of the material during landslide motion (Strom, 2006; Paguican et al., 2014; Dufresne et al., 2016; Collins and Reid, 2019). Where deposits are not reworked by human construction or eroded by rivers, we would expect such molard fields to be mappable for decades to centuries.

The Flat Creek glacier detachments originated in permafrost terrain and involved large amounts of glacier ice. The molards are therefore most likely the result of initially frozen material degrading after deposition. We have no direct measurements of subsurface ice content from the release zone, but ERT measurements near the headwall (Line 1, see Fig. 2) indicated a high ice content below an active layer of around 2 m (Jacquemart et al., 2020, and ERT Line 1 in Appendix B). Additionally, we found ground ice on the east side of West Hill, where Flat Creek was undercutting the original hillslope, confirming that permafrost is widespread (Fig. A3). It is therefore highly plausible that the majority of the mobilized and entrained material was ice-cemented or initiated as debris-rich ice, although it is possible that ice and debris also mixed during transport. We further acknowledge the possibility that transport – and subsequent weathering – of weak bedrock blocks could also form conical debris piles, but question whether such weak rock could remain intact during the violent mass flow, only to disintegrate rapidly upon deposition. Ice is mechanically resistant, but will inevitably melt at lower elevations.

Molards have also been documented at other detachment sites, though it is hard to estimate how ubiquitous they are and whether permafrost presence in the release zone is a prerequisite. At the sites of the Aru and Leñas detachments, both assumed to be permafrost areas, similar molard-like mounds can be made out (see Fig. 3 in Falaschi et al. (2019) and Lei et al. (2021)). At the temperate Kolka glacier, molards are not evident in the images of the main deposit presented in Huggel et al. (2005), Haeberli et al. (2004), or Kotlyakov et al. (2004). However, in this case, the debris backed up in a deep depression, where it blocked the local river. It is possible that a molard field would have formed had the mass flow spread out on less constrained terrain. Kotlyakov et al. (2004) do mention “ant heaps” spread across the former glacier bed, which we interpret as a reference to molards. Molards are not visible at the Amney Machen detachment deposits (Fig. A1 in Paul, 2019), but this is based on a single image of an area which may have been reworked when the local road was rebuilt.

5.1.4. Grain sizes and sediment organization

The matrix-supported, unstratified, and chaotic nature of the detachment deposits may be a consequence of both the source material and the deposition process. Abundant debris-rich ice is visible in post-detachment imagery of the release zone (Fig. 9a), consistent with our permafrost assessment. Blocks of frozen material that degrade after deposition do not provide an opportunity for segregation or sorting of the debris during transport. The abundance of ice in the mass flow can also explain the absence of a coarse-grained carapace overlying a more fine-grained interior, which is typical for rock-avalanche deposits. The ice would have reduced the grain-to-grain interactions during transport, minimizing comminution, and thus prevented the development of a fine-grained interior (Dufresne et al., 2016). We acknowledge, however, that we cannot rule out the possibility that something resembling a coarse-grained carapace may yet develop over time as fines are preferentially washed out of the top layer of the deposit.

Unsorted mass flow deposits have also been attributed to rapid material deposition, and to high particle densities that suppress grain size segregation through particle interlocking (Branney and Kokelaar, 1997; Smith and Lowe, 1991). At Flat Creek, rapid deposition may indeed have impaired sedimentary organization, as seismic data indicate that only six or seven minutes elapsed between detachment and deposition. Suppressed grain sorting by high particle densities may also have been possible: the base of the mass flow would have been relatively rich in debris at the start, crudely retaining the original release structure, with the glacier ice travelling atop the denser, particle-rich bed material. This idea is supported by images of the channel immediately after the 2013 mass flows, that show clean ice deposits along the channel (Jacquemart et al., 2020).

Overall, grain size and orientation can be very persistent sedimentological evidence, but adequate sampling is always challenging. Studies of other detachment deposits would be needed to determine whether glacier detachments consistently produce a disorganized sedimentary structure.

5.1.5. Runout distance

The angle of reach (arctan(H/L)) is commonly used to assess the mobility of mass movements. Kääb et al. (2021) reviewed the mobility of glacier detachments and found that glacier detachments tend to attain angles of reach of 5° to 10°, consistent with the values we presented here (6° and 7° for 2013 and 2015, respectively). These low values (i.e. long runouts, as H/L simultaneously represents the apparent friction coefficient) point to an unexpectedly high mobility (Corominas, 1996; Pudasaini and Miller, 2013; Aaron and McDougall, 2019). By comparison, rock-ice avalanches typically have higher angles of reach (i.e. shorter runouts) of 10° or more (Schneider et al., 2011; Kääb et al., 2021). In fact, if we apply the simplest empirical volume to runout-

distance scaling (Davies, 1982), the Flat Creek Glacier detachments ought to have been around 100 times larger. Differently put, glacier detachment runout distances fall far outside what is expected for terrestrial rock and rock-ice avalanches, attaining runout distances that, at the observed volumes, would be more typical for volcanic or submarine mass flows (Pudasaini and Miller, 2013).

While many theories for high mobility have been proposed (Davies, 1982; Legros, 2002; Friedmann et al., 2006; Davies and McSaveney, 2012), it can be assumed that the water provided by the continuous melt of glacier ice drastically reduced friction (Iverson, 1997; Schneider et al., 2011; Yang et al., 2019; Pudasaini and Krautblatter, 2014; Aaron and McDougall, 2019). Whether this process alone can explain the high mobility remains unclear, but water storage within the glacier bed may offer another important source of water. This is in line with the hypothesis that glacier detachments occur due to a failure within the glacier bed in response to high input and temporary storage of water beneath the glacier (Kääb et al., 2018; Gilbert et al., 2018; Jacquemart et al., 2020; Kääb et al., 2021). This initial reservoir of liquid water at the time of release would help drive high speeds and longer runouts. As long as the river does not remove all traces of the Flat Creek deposits, it is likely that the fall-height to runout-distance ratio will be one of the most discernible indicators of this event, and an important hint for identifying a glacier detachment.

5.1.6. Land-system model

To summarize, we believe that the following features may help identify a glacier detachment deposit in the geologic record, listed in order of least to most persistent. It is important to state that none of these indicators are sufficient on their own, and some may be absent entirely, but if multiple are found, a classification may be possible.

1. Rounded ice boulders cemented by debris-rich ice.
2. Meter-scale thermokarst ponds and straight-edged kettle holes.
3. Areas of differential downwasting.
4. A glacier, especially one that is smaller than expected, or a glacier missing where one might otherwise be expected, upslope of the detachment deposit.
5. Source-proximal clasts embedded in debris and superficially scratched in the direction of flow.
6. Hillslope-scale debris stripes (likely) eroded into the (possibly steep) hillslope.
7. Lateral levees, transverse ridges, and an abundance of isolated or closely-spaced molards.
8. The absence of a coarse-grained carapace.
9. Fine-grained, matrix-supported texture that lacks any obvious grain size segregation, sorting or alignment.
10. Long runouts, with angles of reach of 5° to 10°.

5.2. Distinguishing detachment deposits from other mass-movement deposits

Decades of research on rock avalanche, debris-flow, and glacier-surge deposits has identified characteristics typical to each process (e.g., Sharp, 1985; Major, 1998; Sohn et al., 1999; Evans and Rea, 1999; Kim and Lowe, 2004; Strom, 2006; Kjær et al., 2008; Dufresne and Davies, 2009; Dufresne et al., 2016; Dufresne and Dunning, 2017; Serrano and Martín-Moreno, 2018). Below, we integrate our land-system model from the previous section with this existing knowledge to assess whether glacier detachments can be distinguished from other mass movements in the geologic record. Table 2 provides a graphical summary.

Rock-ice avalanche deposits – by definition a mix of rock and ice (Hungr et al., 2014; Evans and Delaney, 2015; Evans et al., 2021) likely yield deposits that are most similar to those of glacier detachments. Kääb et al. (2021) even argue that glacier detachments result in ice-rock avalanches. Our findings suggest that the morphology and sedimentology of glacier detachment deposits is strongly controlled by the high ice content (an estimate based on published literature suggests >50 % ice). Evidence of high ice content may remain in the resulting deposits as widespread thermokarst features and differential downwasting, formed as large bodies of buried ice melt out. These features, and a catchment that could have held a small to medium size, low-angle valley glacier, can help distinguish glacier detachment deposits from otherwise similar rock-ice avalanche deposits.

The vast fields of molards found at Flat Creek could be misinterpreted as the hummocks often found in landslide and rock avalanche deposits. However, such landslide hummocks are formed by extension and faulting of an initially-cohesive slide block (Strom, 2006; Paguican et al., 2014; Dufresne et al., 2016; Collins and Reid, 2019). As a consequence, their size and density typically decrease with increasing distance from the source (e.g., Paguican et al., 2014; Strom, 2006; Collins and Reid, 2019) and they tend to be elongated in the primary direction of flow (Dufresne and Davies, 2009; Collins and Reid, 2019). This presents a conundrum at Flat Creek, where the molards extend to the very edge of the deposits, with no apparent change in size, density, or geometry. This is even the case on the long, fingering deposits that protrude into the forest, where the forward motion must have greatly outpaced horizontal spreading. Generally speaking, the individual mounds are also smaller than what is reported for rock avalanches (Robinson et al., 2015; Reznichenko et al., 2017; Collins and Reid, 2019).

We believe that these differences are due to the molards at Flat Creek having been formed by post-depositional degradation of ice-cemented debris, debris-rich ice, or ice and debris mixed during transport, rather than extensional faulting of initially-cohesive material. Thus, the shape, size, and spatial distribution of debris mounds can help distinguish detachment deposits from rock-avalanche and landslide deposits. However, it must be acknowledged that molards are also frequently found in rock avalanche deposits originating from permafrost terrain (e.g., Brideau et al., 2009; Milana et al., 2016; Morino et al., 2019), and therefore are not exclusive to glacier detachments.

Grain size distributions and clast orientations may also help distinguish glacier detachment deposits from those of rock avalanches. We detected neither a retention of source stratigraphy (that would indicate purely translational motion of bedrock blocks) nor a superficial carapace of large angular boulders overlying a fine grained interior – both typical (but not necessary) characteristics of rock avalanche deposits (Strom, 2006; Dufresne and Davies, 2009; Shugar and Clague, 2011; Dufresne et al., 2016, 2018). Unlike a rock avalanche, whose material is fragmented and segregated during transport, the debris in the detachments likely began as loose material that was cemented by (or encased in) ice. This would have limited the potential for segregation and organization during transport.

The spatial proximity of many glacier detachments to surging glaciers makes it essential that a detachment deposit can be distinguished from deposits left by glacier surges. Evans and Rea (1999), proposed a land-system model that identifies three distinct zones associated with glacier surges: (1) a downstream zone of thrust-block moraines composed of stacked sequences of folded and sheared proglacial deposits that may contain organic layers, (2) a middle zone of patchy hummocks and kame-and-kettle topography formed by the melt-out of heavily fragmented ice mixed with supra- and subglacial debris, and (3) an upstream zone of deformation tills that evidence the squeezing and injection of subglacial tills into heavily fractured ice at the base of the surging glacier. These three zones accurately describe many of the surging glacier deposits documented around the world (e.g., Sharp, 1985; Kjær et al., 2008; Serrano and Martín-Moreno, 2018), though no one zone is distinctive enough to identify a surging glacier on its own (Evans and Rea, 1999).

We did not find any features at Flat Creek that we believe resemble glacier surge deposits. The thrust-block moraines so typical of glacier surges (a result of the slow and repeated deformation of proglacial

Table 2
Qualitative assessment of the likelihood of each feature in our land-system model being associated with a given mass movement. The likelihood classification can be interpreted either as the likelihood that a mass movement will produce a given feature, or the likelihood that if a certain feature is found, that the deposit can be associated with the respective mass movement. The compilation is based on our interpretation of cited literature.

Indicator/Process	Glacier detachment	Glacier surge	Rock-ice avalanche	Rock avalanche	Debris flow
Ice conglomerates					
Small-scale thermokarst					
Differential downwasting					
Missing glacier					
Scratched debris					
Hillslope scratches					
Lateral levees					
Molards					
Lack of coarse-grained carapace					
Matrix-supported interior					
Long runout (Fahrböschung <10°)		–			

Legend: Very likely | Likely | Possible | Unlikely

debris) are notably absent. Furthermore, the hummocks at Flat Creek are too widespread, and the thermokarst features (kettle holes) too small, in our opinion, to resemble those formed by a surging glacier. Relict glacier ice may also be found in historical deposits of surging glaciers, sometimes heavily fractured by the surge process. However, we do not expect a surge to be capable of reworking ice into rounded, (sub-)meter-scale blocks cemented by debris-rich ice, as we found at Flat Creek.

Finally, the lack of grain size sorting or preferential alignment may be an indicator that can help distinguish detachment deposits from the deposits of coarse-grained debris-flows. Though their deposits can be highly chaotic, clasts in coarse-grained debris-flow deposits often exhibit a preferred orientation, either along flow or perpendicular to it (Major, 1998; Sohn et al., 1999; Kim and Lowe, 2004; Tiranti and Deangeli, 2015;). Similarly, lateral levees are frequently enriched with larger grains, and form when coarser grains are shouldered aside by more liquefied parts of the flow (Hubert and Filipov, 1989; Tiranti et al., 2008; Johnson et al., 2012). None of these features were found at Flat Creek. Instead, we found randomly-oriented clasts in a homogenous, fine-grained matrix. The lack of grain-size sorting in the levees along the edges of the deposit leads us to conclude that they instead formed as a result of sudden deceleration and shearing against the forest. Similarly, unstructured deposits might be formed by mudflows or very fine-grained debris flows (Hungr et al., 2014), highlighting the fact that, like all other features described here, the grain-level structure cannot be interpreted on its own.

Finally, there are many factors that control the characteristics of a glacier detachment deposit, and these also need to be considered when trying to determine the origin of a mass-wasting deposit. The presence of ice in the source material (from both the glacier and permafrost), the involved volumes, and the geology and sedimentology of the release area undoubtedly have a major influence on the final deposit morphology. Upon release, the depositional environment determines the possible landforms. The Flat Creek detachments flowed down a gently-inclined channel that gave way to a large alluvial fan. This is a common setting for glacier detachments (see Kääb et al., 2021 for all known events), but many of the depositional features we described may not form the same way in a confined bedrock channel. Or if they do form, deposits in a confined bedrock channel may be fluvially eroded more rapidly than ones that spread over alluvial fans. Finally, we must acknowledge that very few glacier detachments have yet been described in detail, and therefore we lack a sense of the possible diversity of these events. Even at Flat Creek, the varying volumes, ice contents, runout distances and paths highlight a range of outcomes and possible depositional signatures that we were not able to fully detangle.

5.3. History of the East Site

Our land-system model, combined with the observations and measurements made at the East Site, lead us to reject the hypothesis that the East Site deposit was created by a glacier detachment. For one, the remaining ice that we found in the deposit does not resemble the rounded, reconsolidated ice-conglomerate that we found at Flat Creek. Instead, we interpret the block of intact glacier ice at the center of the deposit as a relict tongue of a debris-covered glacier. Another possibility is that the ice was deposited by a surge of the glacier upstream, which subsequently retreated and separated. However, we would have expected a more broken up appearance of the relict ice (see Section 5.2), possibly combined with more and more distributed thermokarst ponds. The presence of a single, fairly large lake adjacent to the ice block indicates that there was initially one continuous body of ice. Additionally, thrust-block moraines, hummocks, and kame-and-kettle topography are absent, making the surge hypothesis a less likely scenario. However, the presence of ice in the deposit does highlight the longevity of remnant ice in this climate.

Additionally, the morphology of the East Site deposit differs substantially from what we found at Flat Creek. The ridges and furrows are reminiscent of a rock glacier, suggesting that the former glacier tongue may have been connected to a rock glacier complex. Molards – which we believe to be distinctive features of glacier detachments – are absent from the East Site deposit. However, the motion measured on the southeastern part of the deposit also shows that such deposits – regardless of their origin – may creep at substantial rates in this climate.

Such creep may lead to a reorganization of the deposits that could eliminate structures such as densely-packed molards.

As suspected, the grain size distributions per-se do not provide much insight, largely due to the limited number of samples. More samples from the East Site, and more data from other detachment deposits, would be needed to determine the significance of grain size distributions. Finally, the fact that the deposit terminates as oversteepened lobes at the edge of steeper terrain suggests that the emplacement occurred by slow creep, rather than by a catastrophic and highly-mobile mass flow for which we would have expected much larger runout distances.

6. Conclusions

We have described the deposits formed by the Flat Creek glacier detachments and attempted to build a land-system model from these observations. We find that there is no single indicator that can be used to distinguish glacier detachments from rock-avalanches or debris-flows, especially once direct glaciological evidence is missing. Nevertheless, a careful interpretation of all available geomorphic and sedimentologic evidence, interpreted in the landscape context, can reveal the origin of a glacier detachment deposit. Our results suggest that distinguishing glacier detachments from glacier surges may be easier due to the absence of glaciotectonic landforms, especially thrust-block moraines.

Our findings clearly show that careful field investigations are necessary to determine the origin of glacier detachment deposits, though high-resolution elevation data and imagery can provide important insights. Further investigations of other contemporary glacier detachments are necessary to solidify and generalize our understanding of these deposits. Due to their similarities with rock-ice avalanches, glacier detachments should be taken into account when (re-)evaluating mass-wasting deposits. A correct interpretation of the processes that formed such deposits will be essential for both the reconstruction of (paleo-) environmental conditions and for reliable hazard assessments in mountain regions.

Code availability

All code used in this study is available at https://github.com/mjacqu/FlatCreek2.

Data availability

SfM orthomosaics and vector data is currently available at doi: https://doi.org/10.3929/ethz-b-000558233

Video supplement

Video of the 2016 mass flow can be seen at https://youtu.be/Xh23H3QApk8

CRediT authorship contribution statement

MJ designed the study, coordinated the field campaign, carried out all analyses not specifically mentioned in the following, and wrote the manuscript. EW performed out the photo-based grain size analyses. MLeopold carried out the ERT measurements and data processing. MLoso provided logistical field support and helped with data interpretation. LL supported the field investigations, and KT supervised the work. All authors edited and approved the manuscript.

Declaration of competing interest

Mylene Jacquemart reports financial support was provided by NASA.

Mylene Jacquemart reports financial support was provided by Swiss National Science Foundation. Mylene Jacquemart reports financial support was provided by Swiss Federal Institute for Forest Snow and Landscape Research.

Kristy Tiampo reports financial support was provided by NASA.

Fieldwork and logistics were covered by the U.S National Park Service, as was Lia Lajoie (Geoscientists in the Parks program).

Data availability

The data are available on a public repository, are open access, and code is available on github.

Acknowledgements

MJ was funded through the NASA Earth and Space Science Fellowhip (NESSF; grant no. 80NSSC17K0391), the WSL research program Climate Change Impacts on Alpine Mass Movements (CCAMM) and the Swiss National Science Foundation (grant no. 200021_184634). Fieldwork and logistics were covered by the U.S National Park Service, as was LL (Geoscientists in the Parks program). We kindly thank Sam McColl for the highly detailed and constructive review, as well as Achim Beylich for his editorial support and feedback.

Appendix A. Additional field photos

Fig. A1. Deposits of the 2013 mass flow. Photo taken in on 7 July 2015, courtesy Jeff Trop, Bucknell University.

Fig. A2. Deposits of the 2013 mass flow. Photo taken in on 7 July 2015, courtesy Jeff Trop, Bucknell University.

Fig. A3. a) Fluvial undercutting of West Hill. b) Close up of the undercut section that is ice-cemented. c) Close-up of clear ground-ice cementing the original hillslope.

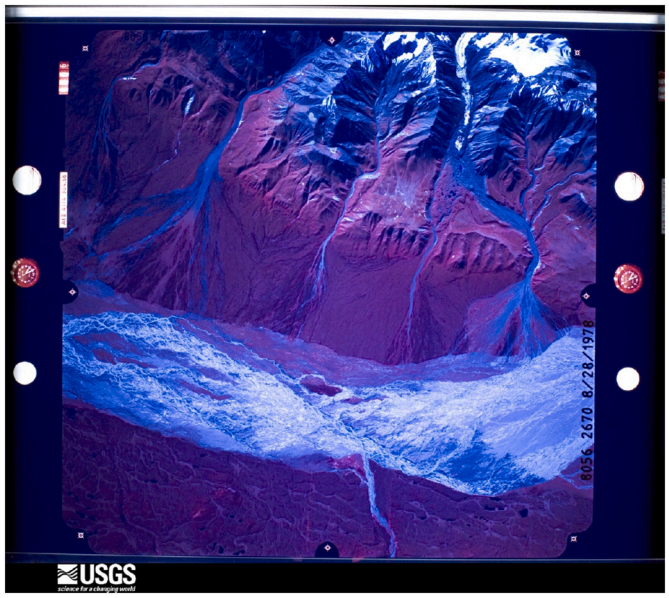

Fig. A4. Alaska High Altitude Photography (AHAP) false-color image of the Flat Creek region from 28 August 1978. Flat Creek is the far left drainage. Various old channels and different stages of vegetation regrowth are visible, indicating that regular debris floods and river avulsions are typical. Image Source: USGS.

Appendix B. Additional ERT data

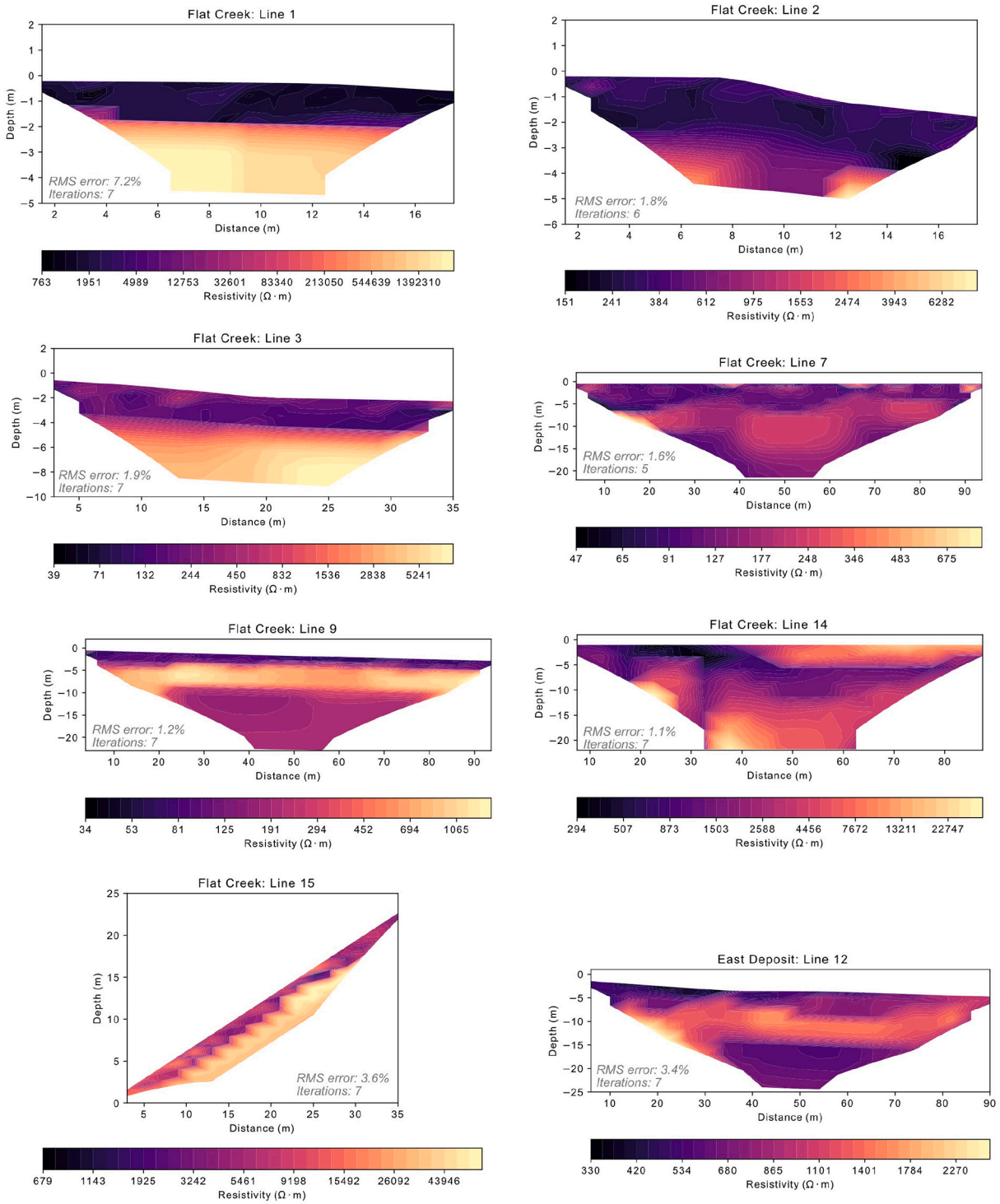

Fig. B1. ERT measurements not presented in main text with brief interpretation. All locations are shown in Fig. 2. Note varying color scales. Line 1: 2 m active layer over ice-rich ground. Line 2: thick deposit near release zone. Line 3: Thick deposits over bedrock or ice-poor permafrost (or both). Line 7: Transect over aggraded river bed showing 5 m to 10 m of highly conductive, freshly aggraded sediment. Line 9: Thin (meter-scale) sediment deposit, likely over older, coarse fluvial deposits with a lower electric conductivity. Line 14: Absence of permafrost on flat areas above the alluvial fan - the higher resistivity areas are likely due to layers of pumice that are found close to the surface in this region (White River Ash; Lerbekmo, 2008). Line 15: North facing transect in steep terrain above the alluvial fan, likely showing low ground ice concentrations and permafrost conditions. Line 12: relatively dry, ice-free conditions on the East Site.

References

Aaron, J., McDougall, S., 2019. Rock avalanche mobility: the role of path material. Eng. Geol. 257, 105126 https://doi.org/10.1016/j.enggeo.2019.05.003.

Benn, D.I., Fowler, A.C., Hewitt, I., Sevestre, H., 2019. A general theory of glacier surges. J. Glaciol. 65, 701–716. https://doi.org/10.1017/jog.2019.62.

Bennett, M.M., Glasser, N.F., 2011. Glacial Geology: Ice Sheets and Landforms. John Wiley & Sons.

Branney, M.J., Kokelaar, P., 1997. Giant bed from a sustained catastrophic density current flowing over topography: Acatlán ignimbrite, Mexico. Geology 25, 115–118. https://doi.org/10.1130/0091-7613(1997)025<0115:GBFASC>2.3.CO;2.

Brideau, M.-A., Stead, D., Lipovsky, P., Jaboyedoff, M., Hopkinson, C., Demuth, M., Barlow, J., Evans, S., Delaney, K., 2009. Preliminary description and slope stability analyses of the 2008 Little Salmon Lake and 2007 Mt. Steele landslides. Yukon 16.

Collins, B.D., Reid, M.E., 2019. Enhanced landslide mobility by basal liquefaction: the 2014 State Route 530 (Oso), Washington, landslide. GSA Bull. 132, 451–476. https://doi.org/10.1130/B35146.1.

Consortium, R.G.I., 2017. Randolph Glacier Inventory – A Dataset of Global Glacier Outlines: Version 6.0: Technical Report, Global Land Ice Measurements from Space, Colorado, USA. Digital Media.

Corominas, J., 1996. The angle of reach as a mobility index for small and large landslides. Can. Geotech. J. 33, 260–271.

Davies, T.R.H., 1982. Spreading of rock avalanche debris by mechanical fluidization. Rock Mech. 15, 9–24.

Davies, T.R.H., McSaveney, M., 2012. Mobility of long-runout landslides. In: Clague, John J., Stead, Douglas (Eds.), Landslides: Types, Mechanisms and Modeling. Cambridge University Press.

Driscoll, F.G., 1980. Wastage of the Klutlan ice-cored moraines, Yukon Territory, Canada 1. Quat. Res. 14, 31–49. https://doi.org/10.1016/0033-5894(80)90005-8.

Dufresne, A., Davies, T.R., 2009. Longitudinal ridges in mass movement deposits. Geomorphology 105, 171–181. https://doi.org/10.1016/j.geomorph.2008.09.009.

Dufresne, A., Dunning, S.A., 2017. Process dependence of grain size distributions in rock avalanche deposits. Landslides 14, 1555–1563. https://doi.org/10.1007/s10346-017-0806-y.

Dufresne, A., Bösmeier, A., Prager, C., 2016. Sedimentology of rock avalanche deposits – Case study and review. Earth Sci. Rev. 163, 234–259. https://doi.org/10.1016/j.earscirev.2016.10.002.

Dufresne, A., Geertsema, M., Shugar, D.H., Koppes, M., Higman, B., Haeussler, P.J., Stark, C., Venditti, J.G., Bonno, D., Larsen, C., Gulick, S.P.S., McCall, N., Walton, M., Loso, M.G., Willis, M.J., 2018. Sedimentology and geomorphology of a large tsunamigenic landslide, Taan Fiord, Alaska. Sediment. Geol. 364, 302–318. https://doi.org/10.1016/j.sedgeo.2017.10.004.

Evans, S.G., Delaney, K.B., 2015. Catastrophic mass flows in the mountain glacial environment. In: Snow and Ice-related Hazards, Risks and Disasters. Elsevier, pp. 563–606.

Evans, D.J.A., Rea, B.R., 1999. Geomorphology and sedimentology of surging glaciers: a land-systems approach. Ann. Glaciol. 28, 75–82. https://doi.org/10.3189/172756499781821823.

Evans, S.G., Tutubalina, O.V., Drobyshev, V.N., Chernomorets, S.S., McDougall, S., Petrakov, D.A., Hungr, O., 2009. Catastrophic detachment and high-velocity long-runout flow of Kolka Glacier, Caucasus Mountains, Russia in 2002. Geomorphology 105, 314–321. https://doi.org/10.1016/j.geomorph.2008.10.008.

Evans, S.G., Delaney, K.B., Rana, N.M., 2021. Chapter 16 - The occurrence and mechanism of catastrophic mass flows in the mountain cryosphere. In: Haeberli, W., Whiteman, C. (Eds.), Snow and Ice-related Hazards, Risks, and Disasters, Second edition. Elsevier, pp. 541–596. https://doi.org/10.1016/B978-0-12-817129-5.00004-4.

Falaschi, D., Kääb, A., Paul, F., Tadono, T., Rivera, J.A., Lenzano, L.E., 2019. Brief communication: Collapse of 4 Mm3 of ice from a cirque glacier in the Central Andes of Argentina. Cryosphere 13, 997–1004. https://doi.org/10.5194/tc-13-997-2019.

Friedmann, S.J., Taberlet, N., Losert, W., 2006. Rock-avalanche dynamics: insights from granular physics experiments. Int. J. Earth Sci. (Geol. Rundsch.) 95, 911–919. https://doi.org/10.1007/s00531-006-0067-9.

Gilbert, A., Leinss, S., Kargel, J., Kääb, A., Gascoin, S., Leonard, G., Berthier, E., Karki, A., Yao, T., 2018. Mechanisms leading to the 2016 giant twin glacier collapses, Aru RangeTibet. The Cryosphere 12, 2883–2900. https://doi.org/10.5194/tc-12-2883-2018.

Glasser, N.F., Hambrey, M.J., 2001. Styles of sedimentation beneath Svalbard valley glaciers under changing dynamic and thermal regimes. J. Geol. Soc. 158, 697–707. https://doi.org/10.1144/jgs.158.4.697.

Haeberli, W., Huggel, C., Kääb, A., Zgraggen-Oswald, S., Polkvoj, A., Galushkin, I., Zotikov, I., Osokin, N., 2004. The Kolka-Karmadon rock/ice slide of 20 September 2002: an extraordinary event of historical dimensions in North Ossetia, Russian Caucasus. J. Glaciol. 50, 533–546. https://doi.org/10.3189/172756504781829710.

Hauck, C., Vonder Mühll, D., 2003. Inversion and interpretation of two-dimensional geoelectrical measurements for detecting permafrost in mountainous regions. Permafr. Periglac. Process. 14, 305–318. https://doi.org/10.1002/ppp.462.

Hubert, J.F., Filipov, A.J., 1989. Debris-flow deposits in alluvial fans on the west flank of the White Mountains, Owens Valley, California, U.S.A. Sediment. Geol. 61, 177–205. https://doi.org/10.1016/0037-0738(89)90057-2.

Huggel, C., Zgraggen-Oswald, S., Haeberli, W., Kääb, A., Polkvoj, A., Galushkin, I., Evans, S.G., 2005. The 2002 rock/ice avalanche at Kolka/Karmadon, Russian Caucasus: assessment of extraordinary avalanche formation and mobility, and application of QuickBird satellite imagery. Nat. Hazards Earth Syst. Sci. 5, 173–187. https://doi.org/10.5194/nhess-5-173-2005.

Hungr, O., Leroueil, S., Picarelli, L., 2014. The Varnes classification of landslide types, an update. Landslides 11, 167–194. https://doi.org/10.1007/s10346-013-0436-y.

Iverson, R.M., 1997. The physics of debris flows. Rev. Geophys. 35, 245–296. https://doi.org/10.1029/97RG00426.

Jacquemart, M., Loso, M., 2019. Catastrophic glacier collapse and debris flow at Flat Creek, Wrangell-St. Elias National Park and Preserve. AlaskaPark. Sci. 18, 10.

Jacquemart, M., Loso, M., Leopold, M., Welty, E., Berthier, E., Hansen, J.S.S., Sykes, J., Tiampo, K., 2020. What drives large-scale glacier detachments? Insights from Flat Creek glacier, St. Elias MountainsAlaska. Geology 48, 703–707. https://doi.org/10.1130/G47211.1.

Johnson, C.G., Kokelaar, B.P., Iverson, R.M., Logan, M., LaHusen, R.G., Gray, J.M.N.T., 2012. Grain-size segregation and levee formation in geophysical mass flows. J. Geophys. Res. 117 https://doi.org/10.1029/2011JF002185.

Kääb, A., Leinss, S., Gilbert, A., Bühler, Y., Gascoin, S., Evans, S.G., Bartelt, P., Berthier, E., Brun, F., Chao, W.-A., Farinotti, D., Gimbert, F., Guo, W., Huggel, C., Kargel, J.S., Leonard, G.J., Tian, L., Treichler, D., Yao, T., 2018. Massive collapse of two glaciers in western Tibet in 2016 after surge-like instability. Nat. Geosci. 11, 114–120. https://doi.org/10.1038/s41561-017-0039-7.

Kääb, A., Jacquemart, M., Gilbert, A., Leinss, S., Girod, L., Huggel, C., Falaschi, D., Ugalde, F., Petrakov, D., Chernomorets, S., Dokukin, M., Paul, F., Gascoin, S., Berthier, E., Kargel, J.S., 2021. Sudden large-volume detachments of low-angle mountain glaciers – more frequent than thought? Cryosphere 15, 1751–1785. https://doi.org/10.5194/tc-15-1751-2021.

Kim, B.C., Lowe, D.R., 2004. Depositional processes of the gravelly debris flow deposits, South Dolomite alluvial fan, Owens Valley, California. Geosci J 8, 153. https://doi.org/10.1007/BF02910191.

Kjær, K.H., Korsgaard, N.J., Schomacker, A., 2008. Impact of multiple glacier surges—a geomorphological map from Brúarjökull, East Iceland. J. Maps 4, 5–20. https://doi.org/10.4113/jom.2008.91.

Kneisel, C., Hauck, C., Fortier, R., Moorman, B., 2008. Advances in geophysical methods for permafrost investigations. Permafr. Periglac. Process. 19, 157–178. https://doi.org/10.1002/ppp.616.

Kotlyakov, V.M., Rototaeva, O.V., Nosenko, G.A., 2004. The September 2002 Kolka Glacier catastrophe in North Ossetia, Russian Federation: evidence and Analysis. Mt. Res. Dev. 24, 78–83. https://doi.org/10.1659/0276-4741(2004)024[0078:TSKGCI]2.0.CO;2.

Krüger, J., Kjær, K.H., 2000. De-icing progression of ice-cored moraines in a humid, subpolar climate, Kötlujökull, Iceland. The Holocene 10, 737–747. https://doi.org/10.1191/09596830094980.

Legros, F., 2002. The mobility of long-runout landslides. Eng. Geol. 63, 301–331. https://doi.org/10.1016/S0013-7952(01)00090-4.

Lei, Y., Yao, T., Tian, L., Sheng, Y., Lazhu, Liao, J., Zhao, H., Yang, W., Yang, K., Berthier, E., Brun, F., Gao, Y., Zhu, M., Wu, G., 2021. Response of downstream lakes to Aru glacier collapses on the western Tibetan Plateau. Cryosphere 15, 199–214. https://doi.org/10.5194/tc-15-199-2021.

Leinss, S., Willimann, C., Hajnsek, I., 2019. Glacier detachment hazard analysis in the West Kunlun Shan Mountains. In: IGARSS 2019 - 2019 IEEE International Geoscience and Remote Sensing Symposium. Presented at the IGARSS 2019 - 2019 IEEE International Geoscience and Remote Sensing Symposium, pp. 4565–4568. https://doi.org/10.1109/IGARSS.2019.8900320.

Leinss, S., Bernardini, E., Jacquemart, M., Dokukin, M., 2021. Glacier detachments and rock-ice avalanches in the Petra Pervogo range, Tajikistan (1973–2019). Nat. Hazards Earth Syst. Sci. 21, 1409–1429. https://doi.org/10.5194/nhess-21-1409-2021.

Leopold, M., Völkel, J., Huber, J., Dethier, D., 2013. Subsurface architecture of the Boulder Creek critical Zone Observatory from electrical resistivity tomography. Earth Surf. Process. Landf. 38, 1417–1431. https://doi.org/10.1002/esp.3420.

Lerbekmo, J.F., 2008. The White River Ash: largest Holocene Plinian tephra. Can. J. Earth Sci. 45, 693–700. https://doi.org/10.1139/E08-023.

Loke, M.H., 2006. RES2DINV ver. 3.55, Rapid 2-D Resistivity & IP Inversion Using the Least-squares Method.

MacKevett Jr., E.M., 1978. Geologic Map of the McCarthy Quadrangle, Alaska (No. 1032). United States Geological Survey.

Major, J.J., 1998. Pebble orientation on large, experimental debris-flow deposits. Sediment. Geol. 117, 151–164. https://doi.org/10.1016/S0037-0738(98)00014-1.

Martin, H.E., Whalley, W.B., 1987. Rock glaciers: part 1: rock glacier morphology: classification and distribution. Prog. Phys. Geogr. Earth Environ. 11, 260–282. https://doi.org/10.1177/030913338701100205.

Milana, J.P., 2016. Molards and their Relation to Landslides Involving Permafrost failure: Molards and permafrost degradation. Permafr. Periglac. Process. 27, 271–284. https://doi.org/10.1002/ppp.1878.

Morino, C., Conway, S.J., Sæmundsson, Þ., Helgason, J.K., Hillier, J., Butcher, F.E.G., Balme, M.R., Jordan, C., Argles, T., 2019. Molards as an indicator of permafrost degradation and landslide processes. Earth Planet. Sci. Lett. 516, 136–147. https://doi.org/10.1016/j.epsl.2019.03.040.

Nuth, C., Kääb, A., 2011. Co-registration and bias corrections of satellite elevation data sets for quantifying glacier thickness change. Cryosphere 5, 271–290. https://doi.org/10.5194/tc-5-271-2011.

Obu, J., Westermann, S., Bartsch, A., Berdnikov, N., Christiansen, H.H., Dashtseren, A., Delaloye, R., Elberling, B., Etzelmüller, B., Kholodov, A., Khomutov, A., Kääb, A., Leibman, M.O., Lewkowicz, A.G., Panda, S.K., Romanovsky, V., Way, R.G., Westergaard-Nielsen, A., Wu, T., Yamkhin, J., Zou, D., 2019. Northern Hemisphere permafrost map based on TTOP modelling for 2000–2016 at 1 km2 scale. Earth Sci. Rev. 193, 299–316. https://doi.org/10.1016/j.earscirev.2019.04.023.

Otsu, N., 1979. A Threshold selection Method from Gray-Level Histograms. IEEE Trans. Syst. Man Cybern. 9, 62–66. https://doi.org/10.1109/TSMC.1979.4310076.

Paguican, E.M.R., van Wyk de Vries, B., Lagmay, A.M.F., 2014. Hummocks: how they form and how they evolve in rockslide-debris avalanches. Landslides 11, 67–80. https://doi.org/10.1007/s10346-012-0368-y.

Paul, F., 2019. Repeat glacier collapses and surges in the Amney Machen mountain range, Tibet, possibly triggered by a developing rock-slope instability. Remote Sens. 11, 708. https://doi.org/10.3390/rs11060708.

Pudasaini, S.P., Krautblatter, M., 2014. A two-phase mechanical model for rock-ice avalanches. J. Geophys. Res. Earth Surf. 119, 2272–2290. https://doi.org/10.1002/2014JF003183.

Pudasaini, S.P., Miller, S.A., 2013. The hypermobility of huge landslides and avalanches. Eng. Geol. 157, 124–132. https://doi.org/10.1016/j.enggeo.2013.01.012.

Reznichenko, N.V., Andrews, G.R., Geater, R.E., Strom, A., 2017. Multiple origins of large hummock deposits in Alai Valley, Northern Pamir: Implications for palaeoclimate reconstructions. Geomorphology 285, 347–362. https://doi.org/10.1016/j.geomorph.2017.02.019.

Robinson, T.R., Davies, T.R.H., Reznichenko, N.V., De Pascale, G.P., 2015. The extremely long-runout Komansu rock avalanche in the Trans Alai range, Pamir Mountains, southern Kyrgyzstan. Landslides 12, 523–535. https://doi.org/10.1007/s10346-014-0492-y.

Scheidegger, A.E., 1973. On the prediction of the reach and velocity of catastrophic landslides. Rock Mech. 5, 231–236.

Schneider, D., Huggel, C., Haeberli, W., Kaitna, R., 2011. Unraveling driving factors for large rock–ice avalanche mobility. Earth Surf. Process. Landf. 36, 1948–1966. https://doi.org/10.1002/esp.2218.

Schomacker, A., Kjær, K.H., 2007. Origin and de-icing of multiple generations of ice-cored moraines at Brúarjökull, Iceland. Boreas 36, 411–425. https://doi.org/10.1080/03009480701213554.

Schomacker, A., Kjær, K.H., 2008. Quantification of dead-ice melting in ice-cored moraines at the high-Arctic glacier Holmströmbreen, Svalbard. Boreas 37, 211–225. https://doi.org/10.1111/j.1502-3885.2007.00014.x.

Schwartz, D.P., Haeussler, P.J., Seitz, G.G., Dawson, T.E., 2012. Why the 2002 Denali fault rupture propagated onto the Totschunda fault: implications for fault branching and seismic hazards. J. Geophys. Res. 117, 25. https://doi.org/10.1029/2011JB008918.

Serrano, E., Martín-Moreno, R., 2018. Surge glaciers during the Little Ice Age in the Pyrenees. CIG 44, 213. https://doi.org/10.18172/cig.3399.

Sevestre, H., Benn, D.I., 2015. Climatic and geometric controls on the global distribution of surge-type glaciers: implications for a unifying model of surging. J. Glaciol. 61, 646–662. https://doi.org/10.3189/2015JoG14J136.

Sharp, M., 1985. Sedimentation and stratigraphy at Eyjabakkajökull—An Icelandic surging glacier. Quat. Res. 24, 268–284. https://doi.org/10.1016/0033-5894(85)90050-X.

Shugar, D.H., Clague, J.J., 2011. The sedimentology and geomorphology of rock avalanche deposits on glaciers. Sedimentology 58, 1762–1783. https://doi.org/10.1111/j.1365-3091.2011.01238.x.

Smith, G.A., Lowe, D.R., 1991. Lahars: volcano hydrologic events and deposition in the debris flow - hyperconcentrated flow continuum. In: Fisher, R.V., Smith, G.A. (Eds.), Sedimentation in Volcanic Settings. SEPM (Society for Sedimentary Geology). https://doi.org/10.2110/pec.91.45.

Sohn, Y.K., Rhee, C.W., Kim, B.C., 1999. Debris flow and hyperconcentrated flood-flow deposits in an Alluvial Fan, northwestern part of the cretaceous Yongdong Basin, central Korea. J. Geol. 107, 111–132. https://doi.org/10.1086/314334.

Stoops, G., 2020. Guidelines for Analysis and Description of Soil and Regolith Thin Sections, 2nd ed. Wiley.

Strom, A., 2006. Morphology and internal structure of rockslides and rock avalanches: grounds and constraints fro their modelling. In: Evans, S.G., Mugnozza, G.S., Strom, A., Hermanns, R.L. (Eds.), Landslides from Massive Rock Slope Failure, NATO Science Series. Springer, Netherlands, Dordrecht, pp. 305–326.

Team, Planet, 2017. Planet Application Program Interface. Space for Life on Earth, San Francisco, CA.

Tiranti, D., Deangeli, C., 2015. Modeling of debris flow depositional patterns according to the catchment and sediment source area characteristics. Frontiers in Earth Science 3.

Tiranti, D., Bonetto, S., Mandrone, G., 2008. Quantitative basin characterisation to refine debris-flow triggering criteria and processes: an example from the Italian Western Alps. Landslides 5, 45–57. https://doi.org/10.1007/s10346-007-0101-4.

Wilson, F.H., Hults, C.P., Mull, C.G., Karl, S.M., 2015. Geologic map of Alaska: U.S. Geological Survey Scientific Investigations Map 3340. In: USGS Numbered Series. Geologic Map of Alaska, Scientific Investigations Map. U.S. Geological Survey, Reston, VA. https://doi.org/10.3133/sim3340.

Yang, Q., Su, Z., Cheng, Q., Ren, Y., Cai, F., 2019. High mobility of rock-ice avalanches: insights from small flume tests of gravel-ice mixtures. Eng. Geol. 260, 105260 https://doi.org/10.1016/j.enggeo.2019.105260.